SIAM J. SCI. COMPUT.
Vol. 42, No. 5, pp. B1136–B1172

A WELL-BALANCED ASYMPTOTIC PRESERVING SCHEME FOR THE TWO-DIMENSIONAL SHALLOW WATER EQUATIONS OVER IRREGULAR BOTTOM TOPOGRAPHY*

XIN LIU†

Abstract. A new well-balanced asymptotic preserving scheme for two-dimensional low Froude number shallow water flows over irregular bottom is developed in this study. The bed-slope terms in the low Froude number regime are nontrivial since their stiffness has the same order as the gravity waves, they change the flow behavior in the low Froude number regime, and thus require special treatment when developing a numerical scheme to ensure such terms will not introduce high order numerical diffusion and spurious waves. To this end, the governing system is reformulated to obtain the well-balanced property. Since the system is stiff in the low Froude number flow regime, conventional explicit numerical schemes are extremely inefficient and often impractical. In order to overcome such difficulties, an asymptotic preserving scheme is developed by splitting the flux into a slow nonlinear part and fast linear part first, then approximating the slow dynamics explicitly using an explicit shock capturing scheme while estimating the fast dynamics implicitly. Using in space the linear piecewise reconstruction with minmod limiter for the shock explicit capturing scheme and central difference method for implicit derivatives, and in time the second order implicit-explicit Runge–Kutta methods, the second order accuracy of the proposed scheme is achieved. It is proved that the proposed numerical schemes are asymptotically consistent and stable uniformly with respect to small Froude number. Several numerical experiments are conducted to demonstrate the performance of the proposed asymptotic preserving numerical methods.

Key words. shallow water equations, asymptotic preserving, well-balanced, flux splitting, implicit-explicit approach, bed-slope term

AMS subject classifications. 76M12, 65M08, 35L65, 86-08, 65M99

DOI. 10.1137/19M1262590

1. Introduction. Oceanographic and atmospheric flows generally take place over horizontal length scales which are much larger than vertical length scale. Accordingly, they can be demonstrated using the shallow water equations (SWEs) which demonstrate a thin layer free surface flow of constant density under hydrostatic assumption over a rigid bottom. Two-dimensional (2D) SWEs over irregular bottom read

$$\begin{aligned} &h_t + (hu)_x + (hv)_y = 0, \\ &(hu)_t + \left(hu^2 + \frac{g}{2}h^2\right)_x + (huv)_y = -ghB_x, \\ &(hv)_t + (huv)_x + \left(hv^2 + \frac{g}{2}h^2\right)_y = -ghB_y, \end{aligned} \tag{1.1}$$

where t is the time, x and y are horizontal spatial coordinates, $h(x, y, t)$ is the water depth, $u(x, y, t)$ and $v(x, y, t)$ are the x- and y-components of the flow velocity, g is the constant gravitational acceleration, and $B(x, y)$ is the bed elevation. The ratio between advection and gravity wave speed can be demonstrated by the Froude number defined by $\mathrm{Fr} := \sqrt{\frac{u^2+v^2}{gh}}$.

*Submitted to the journal's Computational Methods in Science and Engineering section May 20, 2019; accepted for publication (in revised form) June 25, 2020; published electronically September 15, 2020.
https://doi.org/10.1137/19M1262590
†Numerical Environmental Prediction Section, Canadian Meteorological Centre, Environment and Climate Change Canada, Dorval, QC, H9P 1J3, Canada (xliu111@uottawa.ca).

With the dimensionless variables defined by

$$\widehat{x} := \frac{x}{\ell_0}, \quad \widehat{y} := \frac{y}{\ell_0}, \quad \widehat{t} := \frac{t}{t_0}, \quad \widehat{h} := \frac{h}{h_0}, \quad \widehat{u} := \frac{u}{w_0}, \quad \widehat{v} := \frac{v}{w_0}, \quad \widehat{B} := \frac{B}{h_0}, \tag{1.2}$$

using the characteristic length ℓ_0, characteristic time t_0, characteristic depth h_0, and characteristic velocity w_0, one can define the group parameter Strouhal and Froude numbers as

$$\mathrm{Sr} := \frac{\ell_0}{t_0 w_0} \quad \text{and} \quad \mathrm{Fr} := \frac{w_0}{\sqrt{g h_0}}, \tag{1.3}$$

respectively. One can denote by $\varepsilon^{\varrho} = \mathrm{Fr}$ the reference Froude number, with ϱ depending on the particular flow regime considered.

Remark 1.1. Particular distinguished limits of these dimensionless group parameters can define different asymptotic limit regimes for multiscale waves generated in the low Froude number limit. This study focuses on the slower "current-like" processes and asymptotically preserving the wave structures in the scale resolved by the dimensionless coordinate x. Thus it is set $\mathrm{Fr} = \varepsilon$, i.e., $\varrho = 1$, and we obtain $\mathrm{Sr} = 1$ by choosing $t_0 = \ell_0/w_0$.

Accordingly, substituting (1.2) and (1.3) into (1.1) and dropping the hats in the notation for simplicity, one obtains the following dimensionless form of the SWEs:

$$\begin{aligned} &h_t + (hu)_x + (hv)_y = 0, \\ &(hu)_t + \left(hu^2 + \frac{1}{\varepsilon^2}\frac{h^2}{2}\right)_x + (huv)_y = -\frac{1}{\varepsilon^2} h B_x, \\ &(hv)_t + (huv)_x + \left(hv^2 + \frac{1}{\varepsilon^2}\frac{h^2}{2}\right)_y = -\frac{1}{\varepsilon^2} h B_y. \end{aligned} \tag{1.4}$$

When modeling environmental large scale flows using the SWEs, low Froude number flows are typically observed; for example, as described in [31], the typical Froude number ε is around 0.03 in the atmospheric and oceanic flows. The low Froude number leads to a singular limit which is characterized by Fr as the singular parameter approaching zero. The solutions of the SWE system in such singular regimes may suffer major difficulties. The main difficulty is that the type of equations changes its nature from hyperbolic to mixed hyperbolic-elliptic in the low Froude number regime; therefore the limiting solution shows a nonuniform behavior as $\varepsilon \to 0$. To prove the convergence of the solutions of hyperbolic system (1.4) to the hyperbolic-elliptic limiting equation in the regime $\varepsilon \to 0$ is very demanding; see [10, 27, 28, 36, 43].

In addition, approximating such low Froude number shallow water flows numerically also suffers difficulties due to its stiffness. If one divides the spatial domain Ω using Cartesian cells of size $\Delta x \Delta y$ and uses an explicit scheme to numerically solve the system (1.4), the Courant–Friedrichs–Lewy (CFL) condition yields the following stability requirement by limiting the time step size Δt_{ex}:

$$\Delta t_{\mathrm{ex}} \le \mathrm{CFL} \cdot \min\left(\frac{\Delta x}{\max\limits_{u,\eta}\left\{|u| + \frac{1}{\varepsilon}\sqrt{h}\right\}}, \frac{\Delta y}{\max\limits_{v,\eta}\left\{|v| + \frac{1}{\varepsilon}\sqrt{h}\right\}} \right) = \mathcal{O}(\varepsilon \Delta_{\min}), \tag{1.5}$$

where $\Delta_{\min} := \min(\Delta x, \Delta y)$ and $0 < \text{CFL} \leq 1$ is the CFL number. Moreover, numerical diffusion of explicit schemes would typically be proportional to $\varepsilon^{-1}\Delta^2_{\max}$ for a second order numerical method, where $\Delta_{\max} := \max(\Delta x, \Delta y)$; one thus would have to choose the a well-resolved grid with $\Delta x = \mathcal{O}(\varepsilon^{1/2})$ and $\Delta y = \mathcal{O}(\varepsilon^{1/2})$ to prevent the excessive numerical diffusion from dominating the solution (see [13, 20, 21, 41]). Consequently, one has to choose $\Delta t = \mathcal{O}(\varepsilon^{1.5})$ for an explicit numerical scheme. This obviously leads to a significant computational cost (unacceptable most of the time) for explicit schemes when solving the shallow water system (1.4) in the low Froude number flow regime.

In order to overcome such strong restriction of time step size, the fundamental strategy is applying the semi-implicit schemes in which the slow and fast waves are typically approximated explicitly and implicitly, respectively. Such a strategy was first pursued to the best of the author's knowledge in [29], and later in [16, 17, 18, 30, 33, 48, 50]. Considering the well-prepared initial data, and assuming the solution of the hyperbolic partial differential equations (PDEs) (1.4) converges to the solution of the limiting hyperbolic-elliptic PDEs as $\varepsilon \to 0$, the concept of the asymptotic preserving (AP) scheme was introduced in [24] to consider the uniform convergence of the stiff PDE system to its limiting equations in the discrete level in a uniformly stable manner; see also the general reviews in [23, 25]. Specifically, it is accordingly defined in the current study an AP scheme as below.

Definition 1.2. *A numerical scheme is called asymptotic preserving if the discrete numerical scheme is uniformly stable and efficient and provides a consistent discretization of a continuous physical model with singular parameters.*

The AP schemes have been studied for the kinetic equations; see, e.g., [23, 25, 26] and references therein. They have also been developed for the low Mach number Euler and Navier–Stokes equations in [4, 5, 7, 9, 11, 12, 14, 14, 22, 29, 38, 38, 39]. Several AP schemes have been constructed for the shallow water system; see, e.g., [3, 8, 15, 34, 51] for existing results.

The aim of this paper is to develop a well-balanced AP scheme for the SWEs over irregular bottom. In order to obtain the well-balanced property which guarantees all the nontemporal derivatives are exactly balanced and canceled in discrete level at "lake at rest" steady states (2.66), and avoid a complex treatment for the stiff source terms to achieve such a balance, the system (1.4) is reformulated using the free surface variable η instead of h and incorporating part of the bed-slope source term into the flux terms. Accordingly, one only needs to discretize the remaining part of the source term by a simple second order central difference method to obtain the well-balanced property. The AP property is achieved by splitting the reformulated system into a nonstiff part describing slow dynamics and a stiff part modeling fast dynamics, which are treated explicitly and implicitly, respectively. In space, the nonstiff part is discretized by a second order shock capturing scheme based on a piecewise linear reconstruction with minmod limiter, and the stiff part is simply discretized by a second order central difference method. In time, the system is discretized by a second order implicit-explicit (IMEX) Runge–Kutta method. Therefore, the second order accuracy of the proposed AP scheme is obtained.

The reminder of this paper is organized as follows. In section 2, the system is reformulated and the limiting equations in the low Froude regime are derived. Accordingly, a fully discrete AP numerical scheme is developed. Then, the well-balanced property, the uniform consistency, and the uniform stability of the proposed AP method are demonstrated. Several numerical experiments are conducted to investigate the

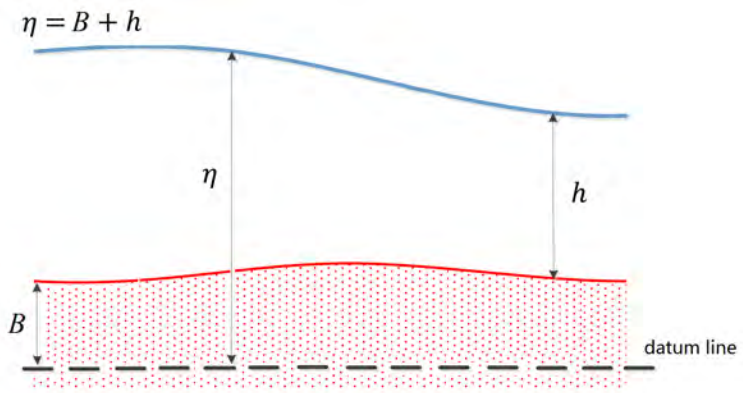

FIG. 1. *Variables of the shallow water system.*

performance of the proposed numerical schemes in section 3. Some concluding remarks complete the paper in section 4.

2. Numerical schemes. This section demonstrates the proposed well-balanced IMEX finite volume schemes for modeling the shallow water flows over the irregular bottom and preserving the asymptotic limit in the low Froude number regime.

2.1. Reformulated governing system. To achieve the well-balanced property, in the current study, we first introduce the water surface variable $\eta = h + B$ and reformulate the system (1.4) as

$$\begin{aligned} &\eta_t + (hu)_x + (hv)_y = 0, \\ &(hu)_t + \left[\frac{(hu)^2}{\eta - B} + \frac{1}{\varepsilon^2}\frac{\eta^2}{2}\right]_x + \left[\frac{(hu)(hv)}{\eta - B}\right]_y = \frac{B}{\varepsilon^2}\eta_x, \\ &(hv)_t + \left[\frac{(hu)(hv)}{\eta - B}\right]_x + \left[\frac{(hv)^2}{\eta - B} + \frac{1}{\varepsilon^2}\frac{\eta^2}{2}\right]_y = \frac{B}{\varepsilon^2}\eta_y. \end{aligned} \tag{2.1}$$

Figure 1 illustrates the free surface η over a rigid bottom B. Notice that η and B are both defined above the datum line in the current study, so that η and B are both nonnegative.

Remark 2.1. The current study is restricted to the case that the shallow water flows over a fully flooded area. Therefore, in order to avoid potential drying process during the wave propagation, it is assumed that the lowest water surface level is always higher than the maximum bed level over the entire domain.

2.2. Low Froude number limiting equations. This section investigates the asymptotic limit of the system (2.1) as $\varepsilon \to 0$. To this end, the formal asymptotic expansions

$$\eta(t,x) = \eta(t,x)^{(0)} + \varepsilon\eta(t,x)^{(1)} + \varepsilon^2\eta(t,x)^{(2)} + \cdots, \tag{2.2}$$

$$h\boldsymbol{u}(t,x) = (h\boldsymbol{u})^{(0)}(t,x) + \varepsilon(h\boldsymbol{u})^{(1)}(t,x) + \varepsilon^2(h\boldsymbol{u})^{(2)}(t,x) + \cdots \tag{2.3}$$

for the unknown variables η and $h\boldsymbol{u} = [hu, hv]^\top$ are substituted into the system (2.1) and the like powers of ε are then collected. Notice that in the following analyses, the dependent symbols (t, x) are dropped for brevity.

Collecting the $\mathcal{O}(\varepsilon^{-2})$ terms, one obtains

$$\eta^{(0)}\nabla\eta^{(0)} = B\nabla\eta^{(0)}, \tag{2.4}$$

which implies $\eta^{(0)}$ is constant in space.

Collecting the $\mathcal{O}(\varepsilon^{-1})$ terms and using $\eta_x^{(0)} = 0$, similarly, one obtains that

$$\eta^{(0)}\nabla\eta^{(1)} = B\nabla\eta^{(1)}, \tag{2.5}$$

which implies $\eta^{(1)}$ is also constant in x. One can accordingly combine $\eta^{(0)}$ and $\varepsilon\eta^{(1)}$ as a constant in space and replace (2.2) by the following formal expansion for surface level:

$$\eta = \eta^{(0)} + \varepsilon^2\eta^{(2)} + \cdots. \tag{2.6}$$

Substituting (2.6) and (2.3) into the system (2.1), and collect the $\mathcal{O}(1)$ terms, one gets that

$$\eta_t^{(0)} + (hu)_x^{(0)} + (hv)_y^{(0)} = 0, \tag{2.7}$$

$$(hu)_t^{(0)} + \left[\frac{[(hu)^{(0)}]^2}{\eta^{(0)} - B} + \eta^{(0)}\eta^{(2)}\right]_x + \left[\frac{(hu)^{(0)}(hv)^{(0)}}{\eta^{(0)} - B}\right]_y = B\eta_x^{(2)}, \tag{2.8}$$

$$(h^{(0)}u^{(0)})_t + \left[\frac{(hu)^{(0)}(hv)^{(0)}}{\eta^{(0)} - B}\right]_x + \left[\frac{[(hv)^{(0)}]^2}{\eta^{(0)} - B} + \eta^{(0)}\eta^{(2)}\right]_y = B\eta_y^{(2)}. \tag{2.9}$$

Integrating (2.7) over the entire flow domain Ω yields

$$-\frac{d\eta^{(0)}}{dt} = \frac{1}{|\Omega|}\int_{\partial\Omega} \nabla\cdot(h\boldsymbol{u})^{(0)}. \tag{2.10}$$

Subjecting to either periodic, wall, or open boundary conditions, or sublinear growth conditions $(\boldsymbol{u}^{(0)}, \eta^0 = \mathrm{o}(|x|), x \to \infty)$, the right-hand side (RHS) of (2.10) is zero and one thus obtains $(\eta^{(0)})_t = 0$ implying that the leading order surface level $\eta^{(0)}$ is constant in both space and time. Accordingly, (2.7) also yields the condition $\nabla\cdot\left(h^{(0)}\boldsymbol{u}^{(0)}\right) = 0$ for the leading order flow discharge.

In summary, one can obtain the zero Froude number limiting equations (also known as the "lake equation")

$$\begin{aligned}
&\eta^{(0)} = \text{Const},\\
&(hu)_x^{(0)} + (hv)_y^{(0)} = 0,\\
&(hu)_t^{(0)} + \left\{\frac{\left[(hu)^{(0)}\right]^2}{\eta^{(0)} - B}\right\}_x + \left[\frac{(hu)^{(0)}(hv)^{(0)}}{\eta^{(0)} - B}\right]_y + (\eta^{(0)} - B)\eta_x^{(2)} = 0,\\
&(hu)_t^{(0)} + \left[\frac{(hu)^{(0)}(hv)^{(0)}}{\eta^{(0)} - B}\right]_x + \left\{\frac{\left[(hv)^{(0)}\right]^2}{\eta^{(0)} - B}\right\}_y + (\eta^{(0)} - B)\eta_y^{(2)} = 0,
\end{aligned} \tag{2.11}$$

which demonstrate the flow behavior of the shallow water approximations over irregular bottom topography in the asymptotic limit.

An AP numerical scheme should yield a consistent approximation of the limiting equations (2.11) as $\varepsilon \to 0$ and preserve the flow behavior described by (2.11) in discrete form.

Remark 2.2. Notice that the limiting equation (2.11) of the reformulated system (2.1) is identical to the classic "lake equation" [6] for original system (1.4) in the asymptotic limit.

2.3. Split system. To construct an AP numerical scheme for the system (2.1), one can first split the fluxes into two parts corresponding to the slow and fast dynamics following the approach in [22] and obtain

$$\eta_t + \alpha(hu)_x + \alpha(hv)_y + (1-\alpha)(hu)_x + (1-\alpha)(hv)_y = 0, \tag{2.12}$$

$$(hu)_t + \left[\frac{(hu)^2}{\eta - B} + \frac{1}{\varepsilon^2}\left(\frac{\eta^2}{2} - a(t)\eta\right)\right]_x + \left[\frac{(hu)(hv)}{\eta - B}\right]_y + \frac{a(t)-B}{\varepsilon^2}\eta_x = 0, \tag{2.13}$$

$$(hv)_t + \left[\frac{(hu)(hv)}{\eta - B}\right]_x + \left[\frac{(hv)^2}{\eta - B} + \frac{1}{\varepsilon^2}\left(\frac{\eta^2}{2} - a(t)\eta\right)\right]_y + \frac{a(t)-B}{\varepsilon^2}\eta_y = 0, \tag{2.14}$$

which can be written in the following vector form:

$$\boldsymbol{U}_t + \widetilde{\boldsymbol{F}}(\boldsymbol{U})_x + \widetilde{\boldsymbol{G}}(\boldsymbol{U})_y + \widehat{\boldsymbol{F}}(\boldsymbol{U}) + \widehat{\boldsymbol{G}}(\boldsymbol{U}) = \boldsymbol{0}, \tag{2.15}$$

where $\boldsymbol{U} := (\eta, hu, hv)^\top$ is the vector of unknown quantities, $\widetilde{\boldsymbol{F}}$ and $\widetilde{\boldsymbol{G}}$ are the x- and y-components of the slow dynamics (nonstiff) parts of the fluxes, respectively,

$$\widetilde{\boldsymbol{F}}(\boldsymbol{U}) := \begin{pmatrix} \alpha hu \\ \dfrac{(hu)^2}{\eta - B} + \dfrac{1}{\varepsilon^2}\left(\dfrac{\eta^2}{2} - a(t)\eta\right) \\ \dfrac{(hu)(hv)}{\eta - B} \end{pmatrix}, \quad \widetilde{\boldsymbol{G}}(\boldsymbol{U}) := \begin{pmatrix} \alpha hv \\ \dfrac{(hu)(hv)}{\eta - B} \\ \dfrac{(hv)^2}{\eta - B} + \dfrac{1}{\varepsilon^2}\left(\dfrac{\eta^2}{2} - a(t)\eta\right) \end{pmatrix}, \tag{2.16}$$

and $\widehat{\boldsymbol{F}}$ and $\widehat{\boldsymbol{G}}$ are the fast dynamics (stiff) parts of the fluxes, respectively,

$$\widehat{\boldsymbol{F}}(\boldsymbol{U}) := \begin{pmatrix} (1-\alpha)(hu)_x \\ \dfrac{a(t)-B}{\varepsilon^2}\eta_x \\ 0 \end{pmatrix}, \quad \widehat{\boldsymbol{G}}(\boldsymbol{U}) := \begin{pmatrix} (1-\alpha)(hv)_y \\ 0 \\ \dfrac{a(t)-B}{\varepsilon^2}\eta_y \end{pmatrix}, \tag{2.17}$$

in which the splitting parameter $0 < \alpha < 1$ determines the proportion of the momentum in slow and fast dynamics parts. In all the following analyses and numerical examples in this study, $\alpha = \varepsilon^2$ is used for low Froude number cases.

Notice that the chosen value of α has to satisfy the condition (2.114) to ensure the stability of the proposed numerical scheme; see the discussion in subsection 2.9. $\alpha = \varepsilon^2$ generally satisfy such a stability condition when $0 < \varepsilon \ll 1$. However, for large Froude number, $\alpha = \varepsilon^2$ may not satisfy (2.114). Therefore, during the computation, it is used that

$$\alpha = \min\left[\varepsilon^2, \frac{1}{2}\min_{j,k}\left(\frac{a-B}{\eta - B}\right)\right]. \tag{2.18}$$

For the subsystem of slow dynamics

$$\boldsymbol{U}_t + \widetilde{\boldsymbol{F}}(\boldsymbol{U})_x + \widetilde{\boldsymbol{G}}(\boldsymbol{U})_y = \boldsymbol{0}, \tag{2.19}$$

the eigenvalues of the Jacobians $\partial\widetilde{\boldsymbol{F}}/\partial\boldsymbol{U}$ and $\partial\widetilde{\boldsymbol{G}}/\partial\boldsymbol{U}$ are

$$\left\{u \pm \sqrt{(1-\alpha)u^2 + \alpha\frac{\eta - a(t)}{\varepsilon^2}},\, u\right\}, \quad \left\{v \pm \sqrt{(1-\alpha)v^2 + \alpha\frac{\eta - a(t)}{\varepsilon^2}},\, v\right\}, \tag{2.20}$$

respectively.

In order to ensure that the subsystem of slow dynamics is nonstiff and hyperbolic, one needs to choose the flux splitting parameters $a(t)$ in an appropriate way to guarantee the eigenvalues (2.20) are real and uniformly bounded with regard to ε, and one can thus avoid the strong stability restriction of the numerical schemes in low Froude number regime.

First, in order to guarantee that all of the eigenvalues in (2.20) are real, it is proposed in the current study to define the spatial constant $a(t)$ as

$$a(t) = \min_{(x,y)\in\Omega} \left(\eta(x,y,t)\right). \tag{2.21}$$

It is noticed that the definition of $a(t)$ (2.21) also guarantees that the eigenvalues (2.20) are independent of the choice of datum line which determines the values of η.

Using the asymptotic expansion (2.6) and (2.21), and using that $\eta^{(0)}$ is constant over the entire domain Ω, one obtains

$$\frac{\eta(x,y,t) - a(t)}{\varepsilon^2} = \left[\eta^{(2)}(x,y,t) - \eta^{(2)}\left(x'(t), y'(t), t\right)\right] = \mathcal{O}(1), \tag{2.22}$$

where $(x'(t), y'(t))$ represent a certain location that $a(t)$ is defined at using (2.21).

Therefore, the subsystem of slow dynamics (2.19) is hyperbolic and its eigenvalues (2.20) are uniformly bounded with respect to ε.

The stability of the subsystem slow dynamics (2.19) is controlled by the CFL condition, which is

$$\Delta t_{AP} \le \mathrm{CFL}_{AP} \cdot \min\left(\frac{\Delta x}{\max\limits_{u,\eta}\left\{|u| + \sqrt{(1-\alpha)u^2 + \alpha\frac{\eta - a(t)}{\varepsilon^2}}\right\}}, \frac{\Delta y}{\max\limits_{v,\eta}\left\{|v| + \sqrt{(1-\alpha)v^2 + \alpha\frac{\eta - a(t)}{\varepsilon^2}}\right\}}\right), \tag{2.23}$$

where $0 < \mathrm{CFL}_{AP} < 1$ is the CFL number for the subsystem of slow dynamics. Given by (2.22), the limiting condition (2.23) is independent of ε so that a large time step of size $\Delta t_{AP} = \mathcal{O}\left(\Delta_{\min}\right)$ can be used when $\varepsilon \to 0$.

2.4. Second order spatial discretization of the split system. In this section, the discretization of derivatives in space is demonstrated. The studied system

(2.15)–(2.17) can be discretized using a finite volume approach in this study. The computational domain is divided into uniform finite volume cells $C_{j,k} = (x_{j-\frac{1}{2}}, x_{j+\frac{1}{2}}) \times (y_{k-\frac{1}{2}}, y_{k+\frac{1}{2}})$, where $x_{j+\frac{1}{2}} - x_{j-\frac{1}{2}} \equiv \Delta x$ and $y_{k+\frac{1}{2}} - y_{k-\frac{1}{2}} \equiv \Delta y$, and it is assumed that the solution at a certain time level $t = t^n$ is available with respect to its cell averages:

$$\overline{\boldsymbol{U}}^n_{j,k} = \frac{1}{\Delta x \Delta y} \iint\limits_{C_{j,k}} \boldsymbol{U}(x, y, t^n)\, \mathrm{d}x\mathrm{d}y.$$

In the rest of this section, the superscript n is dropped since only the discretization in space is demonstrated in this section, and the cell center value $\boldsymbol{U}_{j,k}$ is used to represent the cell averages $\overline{\boldsymbol{U}}^n_{j,k}$ for simplicity.

2.4.1. Numerical discretization of the stiff flux terms. The fast dynamics (stiff) parts (2.17) of the fluxes are treated implicitly in this study. In order to guarantee the second order accuracy in space, the gradients in these stiff parts are discretized using the second order central difference operators

$$\nabla_d \zeta_{j,k} := [D_x \zeta_{j,k}, D_y \zeta_{j,k}]^\top := \left[\frac{\zeta_{j+1,k} - \zeta_{j-1,k}}{2\Delta x}, \frac{\zeta_{j,k+1} - \zeta_{j,k-1}}{2\Delta y}\right]^\top. \tag{2.24}$$

2.4.2. Numerical discretization of the nonstiff flux terms. In each cell, the nonstiff fluxes $\boldsymbol{R}_{j,k} := [R^\eta_{j,k}, R^{hu}_{j,k}, R^{hv}_{j,k}]^\top$

$$\boldsymbol{R}_{j,k} := \Big[\widetilde{\boldsymbol{F}}(\boldsymbol{U})_x\Big]_{j,k} + \Big[\widetilde{\boldsymbol{G}}(\boldsymbol{U})_y\Big]_{j,k} \tag{2.25}$$

are approximated by a finite volume discretization $\boldsymbol{\mathcal{R}}_{j,k} := [\mathcal{R}^\eta_{j,k}, \mathcal{R}^{hu}_{j,k}, \mathcal{R}^{hv}_{j,k}]^\top$,

$$\boldsymbol{\mathcal{R}}_{j,k} := \frac{\widetilde{\boldsymbol{\mathcal{F}}}_{j+\frac{1}{2},k} - \widetilde{\boldsymbol{\mathcal{F}}}_{j-\frac{1}{2},k}}{\Delta x} + \frac{\widetilde{\boldsymbol{\mathcal{G}}}_{j,k+\frac{1}{2}} - \widetilde{\boldsymbol{\mathcal{G}}}_{j,k-\frac{1}{2}}}{\Delta y}, \tag{2.26}$$

where $\widetilde{\boldsymbol{\mathcal{F}}} := [\widetilde{\mathcal{F}}^\eta, \widetilde{\mathcal{F}}^{hu}, \widetilde{\mathcal{F}}^{hv}]^\top$ and $\widetilde{\boldsymbol{\mathcal{G}}} := [\widetilde{\mathcal{G}}^\eta, \widetilde{\mathcal{G}}^{hu}, \widetilde{\mathcal{G}}^{hv}]^\top$ are the Rusanov flux discretization from [42] to approximate $\widetilde{\boldsymbol{F}}$ and $\widetilde{\boldsymbol{G}}$, and their second order format reads

$$\widetilde{\boldsymbol{\mathcal{F}}}_{j+\frac{1}{2},k} = \frac{1}{2}\left[\widetilde{\boldsymbol{F}}(\boldsymbol{U}^{\mathrm{E}}_{j,k}) + \widetilde{\boldsymbol{F}}(\boldsymbol{U}^{\mathrm{W}}_{j+1,k})\right] - \frac{1}{2}\ell^*_{j+\frac{1}{2},k}\left(\boldsymbol{U}^{\mathrm{W}}_{j+1,k} - \boldsymbol{U}^{\mathrm{E}}_{j,k}\right), \tag{2.27}$$

$$\widetilde{\boldsymbol{\mathcal{G}}}_{j,k+\frac{1}{2}} = \frac{1}{2}\left[\widetilde{\boldsymbol{G}}(\boldsymbol{U}^{\mathrm{N}}_{j,k}) + \widetilde{\boldsymbol{G}}(\boldsymbol{U}^{\mathrm{S}}_{j,k+1})\right] - \frac{1}{2}b^*_{j,k+\frac{1}{2}}\left(\boldsymbol{U}^{\mathrm{S}}_{j,k+1} - \boldsymbol{U}^{\mathrm{N}}_{j,k}\right), \tag{2.28}$$

in which $\boldsymbol{U}^{\mathrm{E}}_{j,k}$, $\boldsymbol{U}^{\mathrm{W}}_{j,k}$, $\boldsymbol{U}^{\mathrm{N}}_{j,k}$, and $\boldsymbol{U}^{\mathrm{S}}_{j,k}$ are point values of $\boldsymbol{U}$ at the centers of east, west, north, and south cell interfaces, respectively. They are computed using the following piecewise linear reconstruction:

$$\begin{aligned} \boldsymbol{U}^{\mathrm{E}}_{j,k} &:= \boldsymbol{U}_{j,k} + \frac{\Delta x}{2}(\boldsymbol{U}_x)_{j,k}, \qquad \boldsymbol{U}^{\mathrm{W}}_{j,k} := \boldsymbol{U}_{j,k} - \frac{\Delta x}{2}(\boldsymbol{U}_x)_{j,k}, \\ \boldsymbol{U}^{\mathrm{N}}_{j,k} &:= \boldsymbol{U}_{j,k} + \frac{\Delta y}{2}(\boldsymbol{U}_y)_{j,k}, \qquad \boldsymbol{U}^{\mathrm{S}}_{j,k} := \boldsymbol{U}_{j,k} - \frac{\Delta y}{2}(\boldsymbol{U}_y)_{j,k}. \end{aligned} \tag{2.29}$$

If one uses a constant piecewise reconstruction with that $\boldsymbol{U}_x \equiv \boldsymbol{U}_y \equiv 0$, the approximation (2.27) leads to only first order accuracy in space. In order to obtain

a second order accuracy in space and avoid numerical instability, in the proposed schemes, the slopes $\boldsymbol{U}_x$ and $\boldsymbol{U}_y$ are computed in a nonoscillatory manner using a generalized minmod limiter (see, e.g., [32, 37, 46, 49]),

$$(\boldsymbol{U}_x)_{j,k} = \text{minmod}\left(\theta\,\frac{\boldsymbol{U}_{j+1,k}-\boldsymbol{U}_{j,k}}{\Delta x},\ \frac{\boldsymbol{U}_{j+1,k}-\boldsymbol{U}_{j-1,k}}{2\Delta x},\ \theta\,\frac{\boldsymbol{U}_{j,k}-\boldsymbol{U}_{j-1,k}}{\Delta x}\right), \tag{2.30}$$

with the minmod function

$$\text{minmod}(\phi_1,\phi_2,\ldots) := \begin{cases} \min(\phi_1,\phi_2,\ldots) & \text{if } \phi_i > 0 \ \ \forall i,\\ \max(\phi_1,\phi_2,\ldots) & \text{if } \phi_i < 0 \ \ \forall i,\\ 0 & \text{otherwise.}\end{cases} \tag{2.31}$$

The parameter $\theta \in [1,2]$ in (2.30) controls the amount of numerical dissipation: the larger the θ, the smaller the numerical dissipation. In this paper, $\theta = 2$ is used for all numerical experiments. The limited slope $(\boldsymbol{U}_y)_{j,k}$ can be obtained similarly.

Finally, one can estimate $\ell^*_{j+\frac{1}{2},k}$ and $b^*_{j,k+\frac{1}{2}}$ in (2.27) and (2.28), respectively, from the eigenvalues of the Jacobians $\partial\widetilde{\boldsymbol{F}}/\partial\boldsymbol{U}$ and $\partial\widetilde{\boldsymbol{G}}/\partial\boldsymbol{U}$ as

(2.32)

$$\ell^*_{j+\frac{1}{2},k} = \max\left(\begin{array}{l} \left|\, u^{\mathrm{E}}_{j,k}\,\right| + \sqrt{(1-\alpha)(u^{\mathrm{E}}_{j,k})^2 + \alpha\dfrac{\eta^{\mathrm{E}}_{j,k}-a(t)}{\varepsilon^2}},\\ \qquad\qquad \left|\, u^{\mathrm{W}}_{j+1,k}\,\right| + \sqrt{(1-\alpha)(u^{\mathrm{W}}_{j+1,k})^2 + \alpha\dfrac{\eta^{\mathrm{W}}_{j+1,k}-a(t)}{\varepsilon^2}}\end{array}\right),$$

$$b^*_{j,k+\frac{1}{2}} = \max\left(\begin{array}{l} \left|\, v^{\mathrm{N}}_{j,k}\,\right| + \sqrt{(1-\alpha)(v^{\mathrm{N}}_{j,k})^2 + \alpha\dfrac{\eta^{\mathrm{N}}_{j,k}-a(t)}{\varepsilon^2}},\\ \qquad\qquad \left|\, v^{\mathrm{S}}_{j,k+1}\,\right| + \sqrt{(1-\alpha)(v^{\mathrm{S}}_{j,k+1})^2 + \alpha\dfrac{\eta^{\mathrm{S}}_{j,k+1}-a(t)}{\varepsilon^2}}\end{array}\right).$$

2.5. First order IMEX fully discrete AP schemes. In this section, a first order IMEX fully discrete AP schemes for the split system (2.12)–(2.14) is developed.

First, a first order forward-backward Euler IMEX approach [1] is adopted to relax the strong stability restriction (1.5), the nonstiff flux terms $\widetilde{\boldsymbol{F}}(\boldsymbol{U})_x$ and $\widetilde{\boldsymbol{G}}(\boldsymbol{U})_y$ are approximated explicitly, and the stiff flux terms $\widehat{\boldsymbol{F}}(\boldsymbol{U})$ and $\widehat{\boldsymbol{G}}(\boldsymbol{U})$ are treated implicitly. Accordingly, the split system can be written in the following semi-implicit form:

(2.33a)
$$\frac{\eta^{n+1}-\eta^n}{\Delta t} + \alpha(hu)^n_x + \alpha(hv)^n_y + (1-\alpha)(hu)^{n+1}_x + (1-\alpha)(hv)^{n+1}_y = 0,$$

(2.33b)
$$\frac{(hu)^{n+1}-(hu)^n}{\Delta t} + \left[\frac{(hu)^2}{\eta-B} + \frac{1}{\varepsilon^2}\left(\frac{\eta^2}{2} - a^n\eta\right)\right]^n_x + \left[\frac{(hu)(hv)}{\eta-B}\right]^n_y + \frac{a^n-B}{\varepsilon^2}\eta^{n+1}_x = 0,$$

(2.33c)
$$\frac{(hv)^{n+1}-(hv)^n}{\Delta t} + \left[\frac{(hu)(hv)}{\eta-B}\right]^n_x + \left[\frac{(hv)^2}{\eta-B} + \frac{1}{\varepsilon^2}\left(\frac{\eta^2}{2} - a^n\eta\right)\right]^n_y + \frac{a^n-B}{\varepsilon^2}\eta^{n+1}_y = 0,$$

where the upper indices n and $n+1$ correspond to the current, t^n, and new, $t^{n+1} = t^n + \Delta t$, time levels, respectively, and $a^n = a(t^n)$.

System (2.33a)–(2.33c) can be further rewritten as

$$\eta^{n+1} + \Delta t(1-\alpha)\left[(hu)_x^{n+1} + (hv)_y^{n+1}\right] = \eta^n - \Delta t R^{\eta,n}, \tag{2.34}$$

$$(hu)^{n+1} = (hu)^n - \Delta t R^{hu,n} - \Delta t \frac{a^n}{\varepsilon^2}\eta_x^{n+1} + \frac{\Delta t}{\varepsilon^2} B \eta_x^{n+1}, \tag{2.35}$$

$$(hv)^{n+1} = (hv)^n - \Delta t R^{hv,n} - \Delta t \frac{a^n}{\varepsilon^2}\eta_y^{n+1} + \frac{\Delta t}{\varepsilon^2} B \eta_y^{n+1}. \tag{2.36}$$

As demonstrated in [12], one can first differentiate equations (2.35) and (2.36) with respect to x and y, respectively, then substitute them into (2.34) and finally obtain the following elliptic solver for η^{n+1}:

$$\begin{aligned}\eta^{n+1} - \beta a^n \Delta \eta^{n+1} + \beta \nabla \cdot \left(B\, \nabla \eta^{n+1}\right) = \eta^n - \Delta t R^{\eta,n} \\ - \Delta t(1-\alpha)\left[(hu)_x^n + (hv)_y^n\right] + \Delta t^2 (1-\alpha)(R_x^{hu,n} + R_y^{hv,n}),\end{aligned} \tag{2.37}$$

where

$$\beta = \frac{(\Delta t)^2(1-\alpha)}{\varepsilon^2}. \tag{2.38}$$

Therefore, one can first solve η^{n+1} by (2.37) and then substitute the obtained η^{n+1} into momentum equations (2.35) and (2.36) to obtain $(hu)^{n+1}$ and $(hv)^{n+1}$ explicitly.

Next, a fully discrete method is constructed by applying the spatial discretizations demonstrated in subsection 2.4 to the semi-implicit temporal discretizations (2.37), (2.35), and (2.36). One thus obtains the following fully discrete formulas:

(2.39)

$$\begin{aligned}\eta_{j,k}^{n+1} - \beta a^n \Delta_d\, \eta_{j,k}^{n+1} + \beta\, \nabla_d \cdot \left(B\, \nabla_d\, \eta^{n+1}\right)_{j,k} = \eta_{j,k}^n - \Delta t \mathcal{R}_{j,k}^{\eta,n} \\ - \Delta t(1-\alpha)\left[D_x\ (hu)_{j,k}^n + D_y\ (hv)_{j,k}^n\right] + \Delta t^2(1-\alpha)\left(D_x \mathcal{R}_{j,k}^{hu,n} + D_y \mathcal{R}_{j,k}^{hv,n}\right),\end{aligned}$$

(2.40)

$$(hu)_{j,k}^{n+1} = (hu)_{j,k}^n - \Delta t \mathcal{R}_{j,k}^{hu,n} - \Delta t \frac{a^n}{\varepsilon^2} D_x \eta_{j,k}^{n+1} + \Delta t \frac{B_{j,k}}{\varepsilon^2} D_x \eta_{j,k}^{n+1},$$

(2.41)

$$(hv)_{j,k}^{n+1} = (hv)_{j,k}^n - \Delta t \mathcal{R}_{j,k}^{hv,n} - \Delta t \frac{a^n}{\varepsilon^2} D_y \eta_{j,k}^{n+1} + \Delta t \frac{B_{j,k}}{\varepsilon^2} D_y \eta_{j,k}^{n+1},$$

where the notation for the second order central difference operators is

(2.42)

$$\Delta_d\, \zeta_{j,k} := \frac{\zeta_{j+1,k} - 2\zeta_{j,k} + \zeta_{j-1,k}}{(\Delta x)^2} + \frac{\zeta_{j,k+1} - 2\zeta_{j,k} + \zeta_{j,k-1}}{(\Delta y)^2},$$

(2.43)

$$\begin{aligned}\nabla_d \cdot (B\, \nabla_d\, \zeta)_{j,k} := \frac{B_{j+\frac{1}{2},k}\zeta_{j+1,k} - \left(B_{j-\frac{1}{2},k} + B_{j+\frac{1}{2},k}\right)\zeta_{j,k} + B_{j-\frac{1}{2},k}\zeta_{j-1,k}}{(\Delta x)^2} \\ + \frac{B_{j,k+\frac{1}{2}}\zeta_{j,k+1} - \left(B_{j,k-\frac{1}{2}} + B_{j,k+\frac{1}{2}}\right)\zeta_{j,k} + B_{j,k-\frac{1}{2}}\zeta_{j,k-1}}{(\Delta y)^2},\end{aligned}$$

in which the bed levels at the midpoint of a certain cell interface are simply estimated by averaging the bed levels at the centers of two neighboring cells, e.g.,

$$B_{j+\frac{1}{2},k} = \frac{B_{j,k} + B_{j+1,k}}{2}. \tag{2.44}$$

It is noticed that in the current study, the Gauss–Seidel iterative algorithm is adopted to solve the linear algebra system (2.39).

2.5.1. Solvability of the schemes. In this section, it is shown that there exists a unique solution for the elliptic solver (2.39) and thus for the scheme (2.39)–(2.41). The linear system (2.39) can be first written as the following vector form:

$$[\mathbb{1} + \beta \boldsymbol{\mathcal{A}}]\, \boldsymbol{\eta}^{n+1} = \boldsymbol{\Theta}^n, \tag{2.45}$$

where

$$\boldsymbol{\mathcal{A}} := -a^n \Delta_d + \nabla_d \cdot (\boldsymbol{B}\, \nabla_d), \tag{2.46}$$

$\mathbb{1}$ denotes the identity matrix, and $\boldsymbol{\Theta}^n$ represents all the RHS terms of (2.39).

Letting the boundary conditions be periodic, fixed wall boundary, or extrapolated, one can analyze the nonsingularity of the elliptical solver (2.45) as follows.

If the bottom is constant, the matrix $\boldsymbol{\mathcal{A}}$ is simplified to

$$\boldsymbol{\mathcal{A}} := (B - a^n)\Delta_d, \tag{2.47}$$

and thus $\mathbb{1} + \beta\boldsymbol{\mathcal{A}}$ is always positive-definite and nonsingular. Therefore the system (2.45) has a unique solution when the bottom is flat.

If the bottom topography is nonconstant, using the second order central difference discretization operators (2.42) and (2.43), one can obtain that, for any row of the matrix $\boldsymbol{\mathcal{A}}$, the magnitude of the diagonal entry is equal to the sum of the magnitudes of all the other entries,

$$\begin{aligned} &\left| \frac{2a^n}{(\Delta x)^2} + \frac{2a^n}{(\Delta y)^2} - \frac{B_{j-\frac{1}{2},k} + B_{j+\frac{1}{2},k}}{(\Delta x)^2} - \frac{B_{j,k-\frac{1}{2}} + B_{j,k+\frac{1}{2}}}{(\Delta y)^2} \right| \\ &= \left| \frac{-a^n + B_{j-\frac{1}{2},k}}{(\Delta x)^2} \right| + \left| \frac{-a^n + B_{j+\frac{1}{2},k}}{(\Delta x)^2} \right| + \left| \frac{-a^n + B_{j,k-\frac{1}{2}}}{(\Delta y)^2} \right| + \left| \frac{-a^n + B_{j,k+\frac{1}{2}}}{(\Delta y)^2} \right|, \end{aligned} \tag{2.48}$$

provided Remark 2.1 holds. Therefore, $\mathbb{1} + \beta\boldsymbol{\mathcal{A}}$ is strictly diagonally dominated and positive-definite. Using the Levy–Desplanques theorem [47], the system (2.45) is thus nonsingular, and it has a unique solution.

Substituting such a unique solution of $\eta_{j,k}^{n+1}$ into (2.40) and (2.40) in turn leads to unique solutions of $(hu)_{j,k}^{n+1}$ and $(hv)_{j,k}^{n+1}$ for each computational cell.

2.6. Second order IMEX fully discrete AP schemes. In this section, a second order IMEX fully discrete AP scheme is developed. Notice that the schemes (2.39)–(2.41) are second order accurate in space but only first order accurate in time. One can obtain second order accuracy in time by implementing a two-stage

globally stiffly accurate IMEX Runge–Kutta scheme ARS(2,2,2) (see [1]), which can be described by the following Butcher tableau:

$$
\begin{array}{c|ccc||ccc}
0 & 0 & 0 & 0 & 0 & 0 & 0 \\
\gamma & \gamma & 0 & 0 & 0 & \gamma & 0 \\
1 & 1-\frac{1}{2\gamma} & \frac{1}{2\gamma} & 0 & 0 & 1-\gamma & \gamma \\
\hline
 & 1-\frac{1}{2\gamma} & \frac{1}{2\gamma} & 0 & 0 & 1-\gamma & \gamma
\end{array} \tag{2.49}
$$

where $\gamma = 1 - \frac{\sqrt{2}}{2}$.

The following describes how to implement the second order IMEX Runge–Kutta method (2.49) to the proposed AP schemes (2.39)–(2.41). As (2.49) is a two-staged IMEX Runge–Kutta method, the $(\cdot)^*$ notation for all of the quantities computed at the first stage is introduced.

The first stage of applying the second order IMEX Runge–Kutta time discretization (2.49) to the split system (2.12)–(2.14) can be written as

$$
\frac{\eta^* - \eta^n}{\Delta t} + \gamma R^{\eta,n} + \gamma(1-\alpha)(hu)_x^* + \gamma(1-\alpha)(hv)_y^* = 0, \tag{2.50}
$$

$$
\frac{(hu)^* - (hu)^n}{\Delta t} + \gamma R^{hu,n} + \gamma \frac{a^n}{\varepsilon^2}\eta_x^* - \gamma \frac{B}{\varepsilon^2}\eta_x^* = 0, \tag{2.51}
$$

$$
\frac{(hv)^* - (hv)^n}{\Delta t} + \gamma R^{hv,n} + \gamma \frac{a^n}{\varepsilon^2}\eta_y^* - \gamma \frac{B}{\varepsilon^2}\eta_y^* = 0. \tag{2.52}
$$

Following the steps in subsection 2.5, one can have that

$$
\begin{aligned}
&\eta_{j,k}^* - \gamma^2 \beta a^n \Delta_d \eta_{j,k}^* + \gamma^2 \beta \nabla_d \cdot (B \nabla_d \eta^*)_{j,k} = \eta^n - \gamma \Delta t \mathcal{R}_{j,k}^{\eta,n} \\
&\quad - \gamma \Delta t (1-\alpha)\left[D_x (hu)^n + D_y (hv)^n\right] + \gamma^2 \Delta t^2 (1-\alpha)\left[\left(\mathcal{R}_{j,k}^{hu,n}\right)_x + \left(\mathcal{R}_{j,k}^{hv,n}\right)_y\right],
\end{aligned} \tag{2.53}
$$

$$
(hu)_{j,k}^* = (hu)_{j,k}^n - \gamma \Delta t \mathcal{R}_{j,k}^{hu,n} - \gamma \Delta t \frac{a^n}{\varepsilon^2} D_x \eta_{j,k}^* + \frac{\gamma \Delta t}{\varepsilon^2} B_{j,k} D_x \eta_{j,k}^*, \tag{2.54}
$$

$$
(hv)_{j,k}^* = (hv)_{j,k}^n - \gamma \Delta t \mathcal{R}_{j,k}^{hv,n} - \gamma \Delta t \frac{a^n}{\varepsilon^2} D_y \eta_{j,k}^* + \frac{\gamma \Delta t}{\varepsilon^2} B_{j,k} D_y \eta_{j,k}^*, \tag{2.55}
$$

where β is defined by (2.38). It is noticed that the system (2.53)–(2.55) coincides with the system (2.39)–(2.41) with Δt replaced with $\gamma \Delta t$.

After finding the first stage solutions η^*, $(hu)^*$ and $(hv)^*$ from (2.53)–(2.55), one can continue to apply the second stage of (2.49) to the split system (2.12)–(2.14) and obtain that

$$
\begin{aligned}
&\frac{\eta^{n+1} - \eta^n}{\Delta t} + \frac{1}{2\gamma} R^{\eta,*} + \left(1 - \frac{1}{2\gamma}\right) R^{\eta,n} + \gamma(1-\alpha)\left[(hu)_x^{n+1} + (hv)_y^{n+1}\right] \\
&\qquad + (1-\gamma)(1-\alpha)\left[(hu)_x^* + (hv)_y^*\right] = 0,
\end{aligned} \tag{2.56}
$$

$$\frac{(hu)^{n+1}-(hu)^n}{\Delta t}+\frac{1}{2\gamma}R^{hu,*}+\left(1-\frac{1}{2\gamma}\right)R^{hu,n}+\frac{\gamma a^*}{\varepsilon^2}\eta_x^{n+1}+\frac{(1-\gamma)a^n}{\varepsilon^2}\eta_x^* - \frac{\gamma}{\varepsilon^2}B\eta_x^{n+1}-\frac{(1-\gamma)}{\varepsilon^2}B\eta_x^*=0, \tag{2.57}$$

$$\frac{(hv)^{n+1}-(hv)^n}{\Delta t}+\frac{1}{2\gamma}R^{hv,*}+\left(1-\frac{1}{2\gamma}\right)R^{hv,n}+\frac{\gamma a^*}{\varepsilon^2}\eta_y^{n+1}+\frac{(1-\gamma)a^n}{\varepsilon^2}\eta_y^* - \frac{\gamma}{\varepsilon^2}B\eta_y^{n+1}-\frac{(1-\gamma)}{\varepsilon^2}B\eta_y^*=0, \tag{2.58}$$

where

$$a^*(t)=\min_{(x,y)\in\Omega}\left(\eta^*(x,y,t)\right). \tag{2.59}$$

One can then differentiate (2.57) and (2.58) with respect to x and y, respectively, substitute them into (2.60), and obtain the elliptic equation (2.60) for η^{n+1}. Accordingly, one has the following explicit formulas to solve η^{n+1}, $(hu)^{n+1}$ and $(hv)^{n+1}$:

$$\begin{aligned}\eta^{n+1}&-\beta\gamma^2a^*\Delta\eta^{n+1}+\beta\gamma^2\left[\nabla\cdot\left(B\nabla\eta^{n+1}\right)\right]=\eta^n\\&-\Delta t\gamma(1-\alpha)\left[(hu)_x^n+(hv)_y^n\right]-\Delta t\left(1-\frac{1}{2\gamma}\right)R^{\eta,n}\\&+\Delta t^2\gamma(1-\alpha)\left(1-\frac{1}{2\gamma}\right)\left(R_x^{hu,n}+R_y^{hv,n}\right)\\&-\Delta t(1-\gamma)(1-\alpha)\left[(hu)_x^*+(hv)_y^*\right]+\Delta t^2\frac{(1-\alpha)}{2}\left(R_x^{hu,*}+R_y^{hv,*}\right)\\&-\frac{\Delta t}{2\gamma}R^{\eta,*}+\beta\gamma(1-\gamma)\left[a^n\Delta\eta^*-\nabla\cdot\left(B\nabla\eta^*\right)\right],\end{aligned} \tag{2.60}$$

$$\begin{aligned}(hu)^{n+1}=(hu)^n&-\frac{\Delta t}{2\gamma}R^{hu,*}-\Delta t\left(1-\frac{1}{2\gamma}\right)R^{hu,n}\\&-\Delta t\frac{\gamma a^*}{\varepsilon^2}\eta_x^{n+1}-\Delta t\frac{(1-\gamma)a^n}{\varepsilon^2}\eta_x^*+\Delta t\frac{(1-\gamma)}{\varepsilon^2}B\eta_x^*+\Delta t\frac{\gamma}{\varepsilon^2}B\eta_x^{n+1},\end{aligned} \tag{2.61}$$

$$\begin{aligned}(hv)^{n+1}=(hv)^n&-\frac{\Delta t}{2\gamma}R^{hv,*}-\Delta t\left(1-\frac{1}{2\gamma}\right)R^{hv,n}\\&-\Delta t\frac{\gamma a^*}{\varepsilon^2}\eta_y^{n+1}-\Delta t\frac{(1-\gamma)a^n}{\varepsilon^2}\eta_y^*+\Delta t\frac{(1-\gamma)}{\varepsilon^2}B\eta_y^*+\Delta t\frac{\gamma}{\varepsilon^2}B\eta_y^{n+1}.\end{aligned} \tag{2.62}$$

Computing the nonstiff flux terms $\boldsymbol{R}^n$ and $\boldsymbol{R}^*$ using the finite volume Rusanov discretization $\boldsymbol{\mathcal{R}}_{j,k}^n$ and $\boldsymbol{\mathcal{R}}_{j,k}^*$, and discretizing all the other spatial derivatives in (2.60)–(2.62) using the second-order central differences operators (2.24), (2.42), and (2.43), one obtains the following fully discrete scheme for the elliptic equation (2.60):

$$
\begin{aligned}
(2.63)\qquad & \eta_{j,k}^{n+1} - \beta\gamma^2 a^* \Delta_d\, \eta_{j,k}^{n+1} + \beta\gamma^2 \left[\nabla_d \cdot \left(B \nabla_d \eta^{n+1}\right)_{j,k}\right] = \eta_{j,k}^{n} \\
& - \Delta t \gamma(1-\alpha)\left[D_x\left(hu\right)^n + D_y\left(hv\right)^n\right] - \Delta t\left(1-\frac{1}{2\gamma}\right)\mathcal{R}_{j,k}^{\eta,n} \\
& + \Delta t^2 \gamma(1-\alpha)\left(1-\frac{1}{2\gamma}\right)\left(D_x \mathcal{R}_{j,k}^{hu,n} + D_y \mathcal{R}_{j,k}^{hv,n}\right) \\
& - \Delta t(1-\gamma)(1-\alpha)\left[D_x\left(hu\right)_{j,k}^{*} + D_y\left(hv\right)_{j,k}^{*}\right] \\
& + \Delta t^2 \frac{(1-\alpha)}{2}\left(D_x \mathcal{R}_{j,k}^{hu,*} + D_y \mathcal{R}_{j,k}^{hv,*}\right) - \frac{\Delta t}{2\gamma}\mathcal{R}_{j,k}^{\eta,*} \\
& + \beta\gamma(1-\gamma)\left[a^n \Delta_d\, \eta_{j,k}^{*} - \nabla_d \cdot \left(B \nabla_d \eta^{*}\right)_{j,k}\right].
\end{aligned}
$$

The $\eta_{j,k}^{n+1}$ computed by linear algebra system (2.63) can then be substituted into fully discrete equations (2.61) and (2.62):

$$
\begin{aligned}
(2.64)\qquad (hu)_{j,k}^{n+1} = {} & (hu)_{j,k}^{n} - \frac{\Delta t}{2\gamma}\mathcal{R}_{j,k}^{(hu),*} - \Delta t\left(1-\frac{1}{2\gamma}\right)\mathcal{R}_{j,k}^{(hu),n} - \Delta t \frac{\gamma a^*}{\varepsilon^2} D_x\, \eta_{j,k}^{n+1} \\
& - \Delta t \frac{(1-\gamma)a^n}{\varepsilon^2} D_x\, \eta_{j,k}^{*} + \Delta t \frac{\gamma}{\varepsilon^2} B_{j,k} D_x \eta_{j,k}^{n+1} + \Delta t \frac{(1-\gamma)}{\varepsilon^2} B_{j,k} D_x \eta_{j,k}^{*},
\end{aligned}
$$

$$
\begin{aligned}
(2.65)\qquad (hv)_{j,k}^{n+1} = {} & (hv)_{j,k}^{n} - \frac{\Delta t}{2\gamma}\mathcal{R}_{j,k}^{(hv),*} - \Delta t\left(1-\frac{1}{2\gamma}\right)\mathcal{R}_{j,k}^{(hv),n} - \Delta t \frac{\gamma a^*}{\varepsilon^2} D_y\, \eta_{j,k}^{n+1} \\
& - \Delta t \frac{(1-\gamma)a^n}{\varepsilon^2} D_y\, \eta_{j,k}^{*} + \Delta t \frac{\gamma}{\varepsilon^2} B_{j,k} D_y \eta_{j,k}^{n+1} + \Delta t \frac{(1-\gamma)}{\varepsilon^2} B_{j,k} D_y \eta_{j,k}^{*},
\end{aligned}
$$

to explicitly compute $(hu)_{j,k}^{n+1}$ and $(hv)_{j,k}^{n+1}$.

Remark 2.3. Notice that one can prove that the fully discrete linear elliptic solvers (2.53) and (2.63) are nonsingular and have unique solutions in a similar way as demonstrated in subsection 2.5.

2.7. Well-balanced property of the fully discrete schemes. In this section, the proof of the well-balanced property of the proposed AP scheme is given. Such a desired property guarantees that "lake at rest" steady-state solutions,

$$
(2.66)\qquad \boldsymbol{U} = (C, 0, 0)^{\mathsf{T}}, \quad C = \text{Const},
$$

are exactly preserved using the proposed numerical schemes. For brevity, the proof is given here only for the first order IMEX fully discrete schemes in subsection 2.5. The well-balanced property for the second order IMEX fully discrete schemes in subsection 2.6 can be proved in a similar way.

First, one can substitute the "lake at rest" steady-state solutions (2.66) into the flux approximations (2.27) and (2.28) and obtain the following discrete nonstiff fluxes:

$$
\begin{aligned}
(2.67)\qquad & \widetilde{\mathcal{F}}_{j+\frac{1}{2},k}^{\eta,\,n} = 0, \quad \widetilde{\mathcal{G}}_{j,k+\frac{1}{2}}^{\eta,\,n} = 0, \\
& \widetilde{\mathcal{F}}_{j+\frac{1}{2},k}^{hu,\,n} = \frac{1}{\varepsilon^2}\left(\frac{C^2}{2} - a^n C\right), \quad \widetilde{\mathcal{G}}_{j,k+\frac{1}{2}}^{hu,\,n} = 0, \\
& \widetilde{\mathcal{F}}_{j+\frac{1}{2},k}^{hv,\,n} = 0, \quad \widetilde{\mathcal{G}}_{j,k+\frac{1}{2}}^{hv,\,n} = \frac{1}{\varepsilon^2}\left(\frac{C^2}{2} - a^n C\right).
\end{aligned}
$$

Accordingly, it is easily obtained that the finite volume discretization (2.26) is

$$\boldsymbol{\mathcal{R}}^{n}_{j,k} := \left[\mathcal{R}^{\eta,n}_{j,k}, \mathcal{R}^{hu,n}_{j,k}, \mathcal{R}^{hv,n}_{j,k}\right]^{\top} = [\,0,0,0\,]^{\top}. \tag{2.68}$$

Next, it is demonstrated that the proposed AP scheme (2.39)–(2.41) exactly preserves the "lake at rest" steady-state solutions (2.66).

The fully discrete equation (2.39) for solving $\eta^{n+1}_{j,k}$ is first investigated. Substituting the discretization (2.68) into (2.39), one obtains that

$$\eta^{n+1}_{j,k} - \beta a^{n} \Delta_d\, \eta^{n+1}_{j,k} + \beta\, \nabla_d \cdot \left(B\, \nabla_d\, \eta^{n+1}\right)_{j,k} = \eta^{n}_{j,k}, \tag{2.69}$$

which has a unique solution $\eta^{n+1}_{j,k} \equiv \eta^{n}_{j,k} \equiv C$ due to that the matrix

$$\mathbb{1} - \beta\big[a^{n}\Delta_d - \nabla_d \cdot (\boldsymbol{B}\, \nabla_d\,)\,\big] \tag{2.70}$$

is positive-definite and nonsingular.

Specifically, using a simple fixed-point iteration to solve (2.69) over the whole domain in the current study, in the first iterative step, one solves that

$$\begin{aligned}
&\left[1 + \beta\frac{a^{n} - B_{j+\frac{1}{2},k}}{(\Delta x)^2} + \beta\frac{a^{n} - B_{j-\frac{1}{2},k}}{(\Delta x)^2} + \beta\frac{a^{n} - B_{j,k+\frac{1}{2}}}{(\Delta y)^2} + \beta\frac{a^{n} - B_{j,k-\frac{1}{2}}}{(\Delta y)^2}\right]\eta^{n+1}_{j,k} \\
&\quad - \beta\frac{a^{n} - B_{j+\frac{1}{2},k}}{(\Delta x)^2}C - \beta\frac{a^{n} - B_{j-\frac{1}{2},k}}{(\Delta x)^2}C - \beta\frac{a^{n} - B_{j,k+\frac{1}{2}}}{(\Delta y)^2}C - \beta\frac{a^{n} - B_{j,k-\frac{1}{2}}}{(\Delta y)^2}C = C,
\end{aligned}$$

which in turn yields $\eta^{n+1}_{j,k} = C$ for each cell, and correspondingly leads to

$$\eta^{n+1}_{j,k} \equiv C\,, \tag{2.71}$$

over the entire domain during the whole iteration procedures for solving (2.69).

Finally, substituting (2.71) and (2.68) into (2.40) and (2.41), one obtains

$$\begin{aligned}
(hu)^{n+1}_{j,k} &\equiv (hu)^{n}_{j,k} \equiv 0, \\
(hv)^{n+1}_{j,k} &\equiv (hv)^{n}_{j,k} \equiv 0.
\end{aligned} \tag{2.72}$$

In summary, providing the "lake at rest" steady-state solutions (2.66), one obtains

$$\left[\eta^{n+1}_{j,k}, (hu)^{n+1}_{j,k}, (hv)^{n+1}_{j,k}\right]^{\mathsf{T}} \equiv (C,0,0)^{\mathsf{T}} \tag{2.73}$$

using the proposed fully discrete numerical scheme. This justifies the well-balanced property of the developed numerical methods.

2.8. Asymptotic preserving property: Consistency. In this section, it is demonstrated that the proposed fully discrete numerical schemes yield consistent approximation of the limiting equations (2.11) as $\varepsilon \to 0$. For brevity, the following analyses are presented based on the first order IMEX fully discrete AP schemes in subsection 2.5. One can prove such a property in a similar way for the second order IMEX fully discrete AP schemes in subsection 2.6.

2.8.1. Numerical diffusion of the finite-volume discretization (2.26)–(2.32). We first investigate the leading order of the numerical diffusion introduced by the finite volume discretization (2.26)–(2.32). To this end, the x-directional second order Rusanov flux approximation (2.27) is first analyzed and written as

$$\widetilde{\boldsymbol{\mathcal{F}}}^{n}_{j+\frac{1}{2},k} = \frac{\widetilde{\boldsymbol{F}}(\boldsymbol{U}^{n}_{j,k}) + \widetilde{\boldsymbol{F}}(\boldsymbol{U}^{n}_{j+1,k})}{2} + \boldsymbol{\mathcal{D}}^{n}_{j+\frac{1}{2},k}, \tag{2.74}$$

where

$$\begin{aligned}\boldsymbol{\mathcal{D}}^{n}_{j+\frac{1}{2},k} = \frac{1}{2}\left[\widetilde{\boldsymbol{F}}\left(\boldsymbol{U}^{\mathrm{E},n}_{j,k}\right) + \widetilde{\boldsymbol{F}}\left(\boldsymbol{U}^{\mathrm{W},n}_{j+1,k}\right) - \widetilde{\boldsymbol{F}}(\boldsymbol{U}^{n}_{j,k}) - \widetilde{\boldsymbol{F}}(\boldsymbol{U}^{n}_{j+1,k})\right] \\ - \frac{1}{2}\ell^{*}_{j+\frac{1}{2},k}\left(\boldsymbol{U}^{\mathrm{W},n}_{j+1,k} - \boldsymbol{U}^{\mathrm{E},n}_{j,k}\right)\end{aligned} \tag{2.75}$$

represents the numerical diffusion introduced by the Rusanov discretization and all the terms in (2.75) are computed at time level $t = t^n$. $\boldsymbol{\mathcal{D}} := (\mathcal{D}^{\eta}, \mathcal{D}^{hu}, \mathcal{D}^{hv})^{\top}$ denotes the components of the numerical diffusion introduced by the Rusanov flux (2.27) and (2.28).

The leading order of the numerical diffusion in (2.75) with respect to ε is now computed. The asymptotic expansions for the unknowns in (2.75)

$$\begin{aligned}
&\eta^{n}_{j,k} = \eta^{(0),n}_{j,k} + \varepsilon^2\eta^{(2),n}_{j,k} + \cdots,\\
&\eta^{\mathrm{E},n}_{j,k} = \eta^{\mathrm{E},(0),n}_{j,k} + \varepsilon^2\eta^{\mathrm{E},(2),n}_{j,k} + \cdots,\\
&\eta^{\mathrm{W},n}_{j,k} = \eta^{\mathrm{W},(0),n}_{j,k} + \varepsilon^2\eta^{\mathrm{W},(2),n}_{j,k} + \cdots,\\
&(h\boldsymbol{u})^{n}_{j,k} = (h\boldsymbol{u})^{(0),n}_{j,k} + \varepsilon(h\boldsymbol{u})^{(1),n}_{j,k} + \varepsilon^2(h\boldsymbol{u})^{(2),n}_{j,k} + \cdots,\\
&(h\boldsymbol{u})^{\mathrm{E},n}_{j,k} = (h\boldsymbol{u})^{\mathrm{E},(0),n}_{j,k} + \varepsilon(h\boldsymbol{u})^{\mathrm{E},(1),n}_{j,k} + \varepsilon^2(h\boldsymbol{u})^{\mathrm{E},(2),n}_{j,k} + \cdots,\\
&(h\boldsymbol{u})^{\mathrm{W},n}_{j,k} = (h\boldsymbol{u})^{\mathrm{W},(0),n}_{j,k} + \varepsilon(h\boldsymbol{u})^{\mathrm{W},(1),n}_{j,k} + \varepsilon^2(h\boldsymbol{u})^{\mathrm{W},(2),n}_{j,k} + \cdots
\end{aligned} \tag{2.76}$$

are considered. It is assumed that $\eta^{(0),n}_{j,k} = \eta^{(0),n}\ \forall j,k$, where $\eta^{(0),n} = \mathrm{Const}$, and all the limiting equations (2.11) are satisfied at time t^n. Thus, piecewise linear reconstruction (2.29) yields that $\eta^{\mathrm{E},(0)}_{j,k} = \eta^{\mathrm{W},(0)}_{j,k} = \eta^{(0),n}$. Moreover, with the definition of a^n in (2.21), one can expand

$$a^n = a^{(0),n} + \varepsilon^2 a^{(2),n} + \cdots = \eta^{(0),n} + \varepsilon^2 a^{(2),n} + \cdots, \tag{2.77}$$

where $a^{(0),n}$ and $a^{(2),n}$ are constants at time t^n.

Substituting (2.76) into (2.32), one can easily obtain that $\ell^{*}_{j+\frac{1}{2},k} = \mathcal{O}(1)$ according to the definition (2.21) and analyses in subsection 2.3.

For the first component of the numerical diffusion in (2.75), one obtains

$$\begin{aligned}\mathcal{D}^{\eta,n}_{j+\frac{1}{2},k} = \frac{\alpha}{2}\left[(hu)^{\mathrm{E},(0),n}_{j,k} + (hu)^{\mathrm{W},(0),n}_{j+1,k} - (hu)^{(0),n}_{j,k} - (hu)^{(0),n}_{j+1,k}\right] \\ - \varepsilon^2\frac{\ell^{*,n}_{j+\frac{1}{2},k}}{2}\left(\eta^{\mathrm{W},(2),n}_{j+1,k} - \eta^{\mathrm{E},(2),n}_{j,k}\right)\end{aligned} \tag{2.78}$$

for the leading order approximation. Since it is chosen that $\alpha = \varepsilon^2$ (see subsection 2.3) in the current study, the leading order of $\mathcal{D}^{\eta,n}_{j+\frac{1}{2},k}$ in (2.78) is $\mathcal{O}(\varepsilon^2)$.

Collecting the leading order terms for the second component of the numerical diffusion in (2.74), one obtains

$$\mathcal{D}^{hu,n}_{j+\frac{1}{2},k} = \frac{1}{2}\left[\frac{1}{\varepsilon^2}\left(\frac{\left(\eta^{\mathrm{E},(0),n}_{j,k}\right)^2}{2} - a^{(0),n}\eta^{\mathrm{E},(0),n}_{j,k} + \frac{\left(\eta^{\mathrm{W},(0),n}_{j+\frac{1}{2},k}\right)^2}{2} - a^{(0),n}\eta^{\mathrm{W},(0),n}_{j+\frac{1}{2},k} - \frac{\left(\eta^{(0),n}_{j,k}\right)^2}{2} + a^{(0),n}\eta^{(0),n}_{j,k} - \frac{\left(\eta^{(0),n}_{j+1,k}\right)^2}{2} + a^{(0),n}\eta^{(0),n}_{j+1,k}\right) + \mathcal{O}(1)\right] - \frac{\ell^{*,n}_{j+\frac{1}{2},k}}{2}\left[(hu)^{\mathrm{W},(0),n}_{j+1,k} - (hu)^{\mathrm{E},(0),n}_{j,k}\right], \tag{2.79}$$

in which the $\mathcal{O}(\varepsilon^{-2})$ term can be cancelled using $\eta^{\mathrm{E},(0),n}_{j,k} = \eta^{\mathrm{W},(0),n}_{j,k} = \eta^{(0),n}_{j,k} = \eta^{(0),n} = a^{(0),n}$. Accordingly, the leading order of diffusion $\mathcal{D}^{hu,n}_{j+\frac{1}{2},k}$ in (2.79) is $\mathcal{O}(1)$.

For the third component of the numerical diffusion in (2.74), one has

$$\mathcal{D}^{hv,n}_{j+\frac{1}{2},k} = \frac{1}{2}\left[\frac{(hu)^{\mathrm{E},(0),n}_{j,k}(hv)^{\mathrm{E},(0),n}_{j,k}}{\eta^{\mathrm{E},(0),n}_{j,k} - B_{j+\frac{1}{2},k}} + \frac{(hu)^{\mathrm{W},(0),n}_{j+1,k}(hv)^{\mathrm{W},(0),n}_{j+1,k}}{\eta^{\mathrm{W},(0),n}_{j+1,k} - B_{j+\frac{1}{2},k}} - \frac{(hu)^{(0),n}_{j,k}(hv)^{(0),n}_{j,k}}{\eta^{(0),n}_{j,k} - B_{j,k}} - \frac{(hu)^{(0),n}_{j+1,k}(hv)^{(0),n}_{j+1,k}}{\eta^{(0),n}_{j+1,k} - B_{j+1,k}}\right] - \frac{\ell^{*}_{j+\frac{1}{2},k}}{2}\left[(hv)^{\mathrm{W},(0),n}_{j+1,k} - (hv)^{\mathrm{E},(0),n}_{j,k}\right] \tag{2.80}$$

for the leading order approximation. Therefore, the leading order of $\mathcal{D}^{hv,n}_{j+\frac{1}{2},k}$ in (2.80) is $\mathcal{O}(1)$.

Similarly, for the y-directional Rusanov flux (2.28), one obtains that the leading order of the numerical diffusion is $\mathcal{O}(\varepsilon^2)$ $\mathcal{O}(1)$, and $\mathcal{O}(1)$ for the first, second, and third components, respectively.

Finally, substituting the x- and y-directional Rusanov fluxes into (2.26), one can rewrite the finite volume Rusanov discretization (2.26) as

$$\boldsymbol{\mathcal{R}}^n_{j,k} := D_x\widetilde{\boldsymbol{F}}^n_{j,k} + D_y\widetilde{\boldsymbol{G}}^n_{j,k} + \boldsymbol{\mathcal{Q}}^n_{j,k}, \tag{2.81}$$

where $\boldsymbol{\mathcal{Q}}^n_{j,k} := (\mathcal{Q}^{\eta,n}_{j,k}, \mathcal{Q}^{hu,n}_{j,k}, \mathcal{Q}^{hv,n}_{j,k})^\top$ are numerical diffusion which can be expanded with respect to ε in the following way:

$$\begin{aligned}
\mathcal{Q}^{\eta,n}_{j,k}\left(\Delta^2_{\max}\right) &= \varepsilon^2\mathcal{Q}^{\eta,(2),n}_{j,k},\\
\mathcal{Q}^{hu,n}_{j,k}\left(\Delta^2_{\max}\right) &= \mathcal{Q}^{hu,(0),n}_{j,k} + \varepsilon\mathcal{Q}^{hu,(1),n}_{j,k} + \varepsilon^2\mathcal{Q}^{hu,(2),n}_{j,k} + \cdots,\\
\mathcal{Q}^{hv,n}_{j,k}\left(\Delta^2_{\max}\right) &= \mathcal{Q}^{hv,(0),n}_{j,k} + \varepsilon\mathcal{Q}^{hv,(1),n}_{j,k} + \varepsilon^2\mathcal{Q}^{hv,(2),n}_{j,k} + \cdots.
\end{aligned} \tag{2.82}$$

It should be stressed that all of the terms in this expansion (2.82) are proportional to $\Delta^2_{\max}$ since they are introduced by the second order Rusanov flux discretization in subsection 2.4.2.

Notice that using the analytical results (2.82), one can analyze the numerical diffusion introduced in the fully discretized AP schemes later in subsection 2.8.2 to ensure it does not dominate the computed numerical solutions.

2.8.2. Consistency. In this section, it is shown that the proposed fully discrete schemes (2.39)–(2.41) in the low Froude number limit provide a consistent approximation of the limiting equations (2.11).

For this analysis, we consider the asymptotic expansion

$$\begin{aligned} &\eta_{j,k}^{n} = \eta_{j,k}^{(0),n} + \varepsilon^2 \eta_{j,k}^{(2),n} + \cdots, \\ &(h\boldsymbol{u})_{j,k}^{n} = (h\boldsymbol{u})_{j,k}^{(0),n} + \varepsilon (h\boldsymbol{u})_{j,k}^{(1),n} + \varepsilon^2 (h\boldsymbol{u})_{j,k}^{(2),n} + \cdots, \\ &a^n = a^{(0),n} + \varepsilon^2 a^{(2),n} + \cdots = \eta^{(0),n} + \varepsilon^2 a^{(2),n} + \cdots, \end{aligned} \tag{2.83}$$

which is well-prepared initial data satisfying the low Froude number limits in (2.11) at time level t^n.

Subtracting $(\mathbb{1} + \beta \boldsymbol{\mathcal{A}})\, \boldsymbol{\eta}^{(0),n}$ from both sides of (2.39) and multiplying terms on both sides by $\beta^{-1} = \frac{\varepsilon^2}{(\Delta t)^2(1-\alpha)}$, one obtains

$$\begin{aligned} &\beta^{-1}\left(\eta_{j,k}^{n+1} - \eta_{j,k}^{(0),n}\right) - a^n \Delta_d \left(\eta_{j,k}^{n+1} - \eta_{j,k}^{(0),n}\right) \\ &+ \nabla_d \cdot \left[B\, \nabla_d \left(\eta^{n+1} - \eta^{(0),n}\right)\right]_{j,k} = \beta^{-1}\left(\eta_{j,k}^{n} - \eta_{j,k}^{(0),n}\right) \\ &- \beta^{-1}\Delta t \mathcal{R}_{j,k}^{\eta,n} - \beta^{-1}\Delta t(1-\alpha)\left[D_x\,(hu)_{j,k}^{n} + D_y\,(hv)_{j,k}^{n}\right] \\ &+ \beta^{-1}\Delta t^2(1-\alpha)\left(D_x \mathcal{R}_{j,k}^{hu,n} + D_y \mathcal{R}_{j,k}^{hv,n}\right). \end{aligned} \tag{2.84}$$

Substituting (2.76) and (2.82) into (2.81) and using $\alpha = \varepsilon^2$, one can obtain the finite volume numerical discretizations

$$\boldsymbol{\mathcal{R}}_{j,k}^{n} = \left[\mathcal{R}_{j,k}^{\eta,n},\, \mathcal{R}_{j,k}^{hu,n},\, \mathcal{R}_{j,k}^{hv,n}\right]^{\top} = \left[\mathcal{O}(\varepsilon^2),\, \mathcal{O}(1),\, \mathcal{O}(1)\right]^{\top}. \tag{2.85}$$

Substituting (2.85) into (2.84), and using that $\beta^{-1} = \mathcal{O}(\varepsilon^2)$, leads to

$$\left(\beta^{-1} I + \mathcal{A}\right)\left(\eta_{j,k}^{n+1} - \eta_{j,k}^{(0),n}\right) = \mathcal{O}(\varepsilon^2), \tag{2.86}$$

where $\left(\beta^{-1} I + \mathcal{A}\right)$ is positive-definite and nonsingular (with eigenvalues bounded away from zero independently of ε) as proved in subsection 2.5. It thus implies that

$$\eta_{j,k}^{n+1} = \eta^{(0),n} + \mathcal{O}(\varepsilon^2) \tag{2.87}$$

and that

$$\eta_{j,k}^{(0),n+1} = \eta^{(0),n} = \text{Const}. \tag{2.88}$$

Substituting (2.83), (2.85), and (2.87) into (2.40) and (2.41) gives that

$$(hu)_{j,k}^{n+1} = (hu)_{j,k}^{(0),n+1} + \mathcal{O}(\varepsilon), \quad (hv)_{j,k}^{n+1} = (hv)_{j,k}^{(0),n+1} + \mathcal{O}(\varepsilon).$$

Therefore, the solutions at time level $t = t^{n+1}$ can be expanded with respect to ε as

$$\begin{aligned} &\eta_{j,k}^{n+1} = \eta_{j,k}^{(0),n+1} + \varepsilon^2 \eta_{j,k}^{(2),n+1} + \cdots, \\ &(h\boldsymbol{u})_{j,k}^{n+1} = (h\boldsymbol{u})_{j,k}^{(0),n+1} + \varepsilon (h\boldsymbol{u})_{j,k}^{(1),n+1} + \varepsilon^2 (h\boldsymbol{u})_{j,k}^{(2),n+1} + \cdots. \end{aligned} \tag{2.89}$$

Next, one can substitute (2.89), (2.83), (2.81), and (2.82) into (2.39)–(2.41) and collect like powers to show that the fully discrete scheme provides a consistent approximation of the limiting system (2.11) as $\varepsilon \to 0$.

Collecting the $\mathcal{O}(\varepsilon^{-2})$ terms and using that $\eta_{j,k}^{(0),n}$ is a constant in space, one obtains

$$\begin{aligned} &\nabla_d \cdot \left(B \, \nabla_d \, \eta^{(0),n+1} \right)_{j,k} = a^{(0),n} \Delta_d \, \eta_{j,k}^{(0),n+1}, \\ &B_{j,k} D_x \eta_{j,k}^{n+1} = a^n D_x \eta_{j,k}^{n+1}, \qquad B_{j,k} D_y \eta_{j,k}^{n+1} = a^n D_y \eta_{j,k}^{n+1}, \end{aligned} \tag{2.90}$$

which again indicates that $\eta_{j,k}^{(0),n+1} = \eta_{j,k}^{(0),n} = \text{Const}$ as in (2.88).

Collecting the $\mathcal{O}(1)$ terms for the fully discrete momentum equations (2.40) and (2.41), one obtains that

$$\begin{aligned} &\frac{(hu)_{j,k}^{(0),n+1} - (hu)_{j,k}^{(0),n}}{\Delta t} + D_x \left[\frac{\left((hu)_{j,k}^{(0),n} \right)^2}{\eta_{j,k}^{(0),n} - B_{j,k}} \right] + D_y \left[\frac{(hu)_{j,k}^{(0),n} (hv)_{j,k}^{(0),n}}{\eta_{j,k}^{(0),n} - B_{j,k}} \right] \\ &\qquad + (a^{(0),n} - B_{j,k}) D_x \eta_{j,k}^{(2),n+1} = -\mathcal{Q}_{j,k}^{hu,n}, \end{aligned} \tag{2.91}$$

$$\begin{aligned} &\frac{(hv)_{j,k}^{(0),n+1} - (hv)_{j,k}^{(0),n}}{\Delta t} + D_y \left[\frac{\left((hv)_{j,k}^{(0),n} \right)^2}{\eta_{j,k}^{(0),n} - B_{j,k}} \right] + D_x \left[\frac{(hu)_{j,k}^{(0),n} (hv)_{j,k}^{(0),n}}{\eta_{j,k}^{(0),n} - B_{j,k}} \right] \\ &\qquad + (a^{(0),n} - B_{j,k}) D_y \eta_{j,k}^{(2),n+1} = -\mathcal{Q}_{j,k}^{hv,n}. \end{aligned} \tag{2.92}$$

Because the numerical diffusions $\mathcal{Q}_{j,k}^{hu,n}$ and $\mathcal{Q}_{j,k}^{hv,n}$ introduced by Rusanov flux approximation (2.81) are $\mathcal{O}(\Delta_{\max}^2)$, the numerical discretizations (2.91) and (2.92) are consistent discretizations of the third and fourth limiting equations in (2.11), respectively.

Computing the central difference derivative D_x for (2.91) and D_y for (2.92), then substituting them into the collected $\mathcal{O}(1)$ terms for continuity equation (2.39), one obtains that

$$\begin{aligned} &\frac{1}{\Delta t(1-\alpha)} \eta_{j,k}^{(0),n+1} - \Delta t a^{(2),n} \Delta_d \, \eta_{j,k}^{(0),n+1} - \Delta t a^{(0),n} \Delta_d \, \eta_{j,k}^{(2),n+1} \\ &\quad - \Delta t \nabla_d \cdot \left(B \, \nabla_d \, \eta^{(2),n+1} \right)_{j,k} = \frac{1}{\Delta t(1-\alpha)} \eta_{j,k}^{(0),n} \\ &\quad - \Delta t D_x (a^{(0),n} - B_{j,k}) D_x \eta_{j,k}^{(2),n+1} - \Delta t D_y (a^{(0),n} - B_{j,k}) D_y \eta_{j,k}^{(2),n+1} \\ &\quad - D_x (hu)_{j,k}^{(0),n+1} - D_y (hv)_{j,k}^{(0),n+1}. \end{aligned} \tag{2.93}$$

Using that $\eta_{j,k}^{(0),n+1} = \eta_{j,k}^{(0),n} = a^{(0),n} = \text{Const}$, (2.93) can be simplified to

$$D_x (hu)_{j,k}^{(0),n+1} + D_y (hv)_{j,k}^{(0),n+1} = \frac{\eta_{j,k}^{(0),n+1} - \eta_{j,k}^{(0),n}}{\Delta t(1-\alpha)} = 0. \tag{2.94}$$

In summary, the proposed fully discrete numerical schemes (2.39)–(2.41) yield the fully discrete limiting equations

$$
\begin{aligned}
&\eta_{j,k}^{(0),n+1} = \text{Const},\\
&D_x(hu)_{j,k}^{(0),n+1} + D_y(hv)_{j,k}^{(0),n+1} = 0,\\
&\frac{(hu)_{j,k}^{(0),n+1} - (hu)_{j,k}^{(0),n}}{\Delta t} + D_x\left[\frac{\left((hu)_{j,k}^{(0),n}\right)^2}{\eta_{j,k}^{(0),n} - B_{j,k}}\right] + D_y\left[\frac{(hu)_{j,k}^{(0),n}(hv)_{j,k}^{(0),n}}{\eta_{j,k}^{(0),n} - B_{j,k}}\right]\\
&\qquad + (a^{(0),n} - B_{j,k})D_x\eta_{j,k}^{(2),n+1} = -\mathcal{Q}_{j,k}^{hu,n},\\
&\frac{(hv)_{j,k}^{(0),n+1} - (hv)_{j,k}^{(0),n}}{\Delta t} + D_y\left[\frac{\left((hv)_{j,k}^{(0),n}\right)^2}{\eta_{j,k}^{(0),n} - B_{j,k}}\right] + D_x\left[\frac{(hu)_{j,k}^{(0),n}(hv)_{j,k}^{(0),n}}{\eta_{j,k}^{(0),n} - B_{j,k}}\right]\\
&\qquad + (a^{(0),n} - B_{j,k})D_y\eta_{j,k}^{(2),n+1} = -\mathcal{Q}_{j,k}^{hv,n},
\end{aligned}
\tag{2.95}
$$

which are consistent discrete approximations of the limiting system (2.11) in the low Froude number limit.

2.9. Asymptotic preserving property: Stability. This section investigates the stability of the IMEX split system (2.15)–(2.17) based on the notions in [44, 52]. For brevity, it is assumed that the constant linear reconstruction for nonstiff flux approximation is applied, i.e., $(\boldsymbol{U}_x)_{j,k}^n \equiv (\boldsymbol{U}_y)_{j,k}^n \equiv 0\ \forall j,k$ in (2.29).

The split system is first written in the vector form

$$
\boldsymbol{U}_t + J\boldsymbol{U}_x + P\boldsymbol{U}_y = \boldsymbol{U}_t + \left(\widetilde{J} + \widehat{J}\right)\boldsymbol{U}_x + \left(\widetilde{P} + \widehat{P}\right)\boldsymbol{U}_y = \boldsymbol{0},
\tag{2.96}
$$

where the split matrices are

$$
\begin{aligned}
&\widetilde{J}(\boldsymbol{U}) := \begin{bmatrix} 0 & \alpha & 0\\ -\frac{(hu)^2}{(\eta-B)^2} + \frac{\eta-a(t)}{\varepsilon^2} & \frac{2(hu)}{\eta-B} & 0\\ -\frac{(hu)(hv)}{(\eta-B)^2} & \frac{(hv)}{\eta-B} & \frac{(hu)}{\eta-B}\end{bmatrix}, \quad \widehat{J} := \begin{bmatrix} 0 & 1-\alpha & 0\\ \frac{a(t)-B}{\varepsilon^2} & 0 & 0\\ 0 & 0 & 0\end{bmatrix},\\
&\widetilde{P}(\boldsymbol{U}) := \begin{bmatrix} 0 & 0 & \alpha\\ -\frac{(hu)(hv)}{(\eta-B)^2} & \frac{(hv)}{\eta-B} & \frac{(hu)}{\eta-B}\\ -\frac{(hu)^2}{(\eta-B)^2} + \frac{\eta-a(t)}{\varepsilon^2} & 0 & \frac{2(hv)}{\eta-B}\end{bmatrix}, \quad \widehat{P} := \begin{bmatrix} 0 & 0 & 1-\alpha\\ 0 & 0 & 0\\ \frac{a(t)-B}{\varepsilon^2} & 0 & 0\end{bmatrix}.
\end{aligned}
\tag{2.97}
$$

Using the definition of $a(t)$ and analyses in subsection 2.3, one can conclude that

(i) the matrices $\widetilde{J}$, $\widetilde{P}$, $\widehat{J}$, and $\widehat{P}$ all induce hyperbolic systems, respectively;

(ii) the eigenvalues of $\widetilde{J}$ and $\widetilde{P}$ are $\mathcal{O}(1)$ and bounded independently on ε. At least one of the eigenvalues of $\widehat{J}$ and at least one of the eigenvalues of $\widehat{P}$ are $\mathcal{O}(\varepsilon^{-1})$, respectively.

Provided the above conditions hold, the splittings $J = \widetilde{J} + \widehat{J}$ and $P = \widetilde{P} + \widehat{P}$ are admissible according to the definition in [44].

Substituting the spatial descretizations adopted in subsection 2.4, the first order IMEX scheme in subsection 2.5 can be written as

$$\begin{aligned}\boldsymbol{U}_{j,k}^{n+1} = \boldsymbol{U}_{j,k}^{n} &- \frac{\Delta t}{\Delta x}\left(\widetilde{\boldsymbol{\mathcal{F}}}_{j+\frac{1}{2},k}^{n} - \widetilde{\boldsymbol{\mathcal{F}}}_{j-\frac{1}{2},k}^{n} + \widehat{\boldsymbol{\mathcal{F}}}_{j+\frac{1}{2},k}^{n+1} - \widehat{\boldsymbol{\mathcal{F}}}_{j-\frac{1}{2},k}^{n+1}\right) \\ &- \frac{\Delta t}{\Delta y}\left(\widetilde{\boldsymbol{\mathcal{G}}}_{j,k+\frac{1}{2}}^{n} - \widetilde{\boldsymbol{\mathcal{G}}}_{j,k-\frac{1}{2}}^{n} + \widehat{\boldsymbol{\mathcal{G}}}_{j,k+\frac{1}{2}}^{n+1} - \widehat{\boldsymbol{\mathcal{G}}}_{j,k-\frac{1}{2}}^{n+1}\right),\end{aligned} \tag{2.98}$$

in which

$$\widetilde{\boldsymbol{\mathcal{F}}}_{j+\frac{1}{2},k}^{n} = \frac{1}{2}\widetilde{J}\left(\boldsymbol{U}_{j,k}^{n} + \boldsymbol{U}_{j+1,k}^{n}\right) - \frac{\ell_{j+\frac{1}{2},k}^{*}}{2}\left(\boldsymbol{U}_{j+1,k}^{n} - \boldsymbol{U}_{j,k}^{n}\right), \tag{2.99}$$

$$\widehat{\boldsymbol{\mathcal{F}}}_{j+\frac{1}{2},k}^{n+1} = \frac{1}{2}\widehat{J}\left(\boldsymbol{U}_{j,k}^{n+1} + \boldsymbol{U}_{j+1,k}^{n+1}\right). \tag{2.100}$$

Using (2.98)–(2.100), one can write the modified equation of (2.96) at position (x_j, y_k, t^n) as

$$\begin{aligned}\boldsymbol{U}_t + JD_x\boldsymbol{U} + PD_y\boldsymbol{U} = &\frac{\Delta t}{2}\left[\frac{\ell^*\Delta x}{\Delta t}\boldsymbol{I} - \widetilde{J}^2 + \widehat{J}^2 + \left(\widehat{J}\widetilde{J} - \widetilde{J}\widehat{J}\right)\right] D_xD_x\boldsymbol{U} \\ &+ \frac{\Delta t}{2}\left[\frac{b^*\Delta y}{\Delta t}\boldsymbol{I} - \widetilde{P}^2 + \widehat{P}^2 + \left(\widehat{P}\widetilde{P} - \widetilde{P}\widehat{P}\right)\right] D_yD_y\boldsymbol{U},\end{aligned} \tag{2.101}$$

where $\widehat{J}\widetilde{J} - \widetilde{J}\widehat{J}$ and $\widehat{P}\widetilde{P} - \widetilde{P}\widehat{P}$ are the commutators of the stiff and nonstiff Jacobians in the x- and y-directions, respectively. For more details to derive such a modified equation (2.101), interested readers are referred to the proof of Theorem 1 in [44].

Applying the Fourier transform to (2.101), one can obtain the following system linearized around an arbitrarily given state $[\eta, (h\mu)] = [\eta_0, (h\mu)_0]$ in Fourier variables $\hat{\boldsymbol{U}}(x, y, t)$:

$$\hat{\boldsymbol{U}}_t + \mathcal{P}(\xi)\hat{\boldsymbol{U}} + \mathcal{S}(\mu)\hat{\boldsymbol{U}} = \boldsymbol{0}, \tag{2.102}$$

where ξ and μ denote the frequency variables, and the frequency matrices $\mathcal{P}(\xi)$ and $\mathcal{S}(\mu)$ are

$$\begin{aligned}\mathcal{P}(\xi) &:= -i\xi J - \xi^2\mathcal{E}_J, \\ \mathcal{S}(\mu) &:= -i\mu P - \mu^2\mathcal{E}_P,\end{aligned} \tag{2.103}$$

where

$$\begin{aligned}\mathcal{E}_J &:= \frac{\Delta t}{2}\left[\frac{\ell^*\Delta x}{\Delta t}\boldsymbol{I} - \widetilde{J}^2 + \widehat{J}^2 + \left(\widehat{J}\widetilde{J} - \widetilde{J}\widehat{J}\right)\right], \\ \mathcal{E}_P &:= \frac{\Delta t}{2}\left[\frac{b^*\Delta y}{\Delta t}\boldsymbol{I} - \widetilde{P}^2 + \widehat{P}^2 + \left(\widehat{P}\widetilde{P} - \widetilde{P}\widehat{P}\right)\right].\end{aligned} \tag{2.104}$$

According to Corollary 1 in [44], the modified equation (2.101) is L_2-stable if the frequency matrices $\mathcal{P}(\xi)$ and $\mathcal{S}(\mu)$ only have eigenvalues with negative real parts. In this case one can call $\mathcal{P}(\xi)$ and $\mathcal{S}(\mu)$ stable matrices. This implies that one needs to prove the positivity of $\mathcal{E}_J$ and $\mathcal{E}_P$ in order to guarantee the proposed IMEX scheme is stable.

By construction, J and P are hyperbolic and can be diagonalized as $J = V\Lambda_J V^{-1}$ and $P = K\Lambda_P K^{-1}$, respectively, where V and K are the matrix of eigenvectors. Substituting these into (2.103), because similarity transformations do not change the spectrum, one can study the eigenvalues of $\mathring{\mathcal{P}}(\xi)$ and $\mathring{\mathcal{S}}(\mu)$ instead of $\mathcal{P}(\xi) = V\mathring{\mathcal{P}}(\xi)V^{-1}$ and $\mathcal{S}(\mu) = K\mathring{\mathcal{S}}(\mu)K^{-1}$, respectively. $\mathring{\mathcal{P}}(\xi)$ and $\mathring{\mathcal{S}}(\mu)$ are defined as

$$\begin{aligned}\mathring{\mathcal{P}}(\xi) :&= -i\xi\Lambda_J - \xi^2\mathring{\mathcal{E}}_J \\ &= -i\xi\Lambda_J - \xi^2\left[V^{-1}\frac{\ell^*\Delta x}{2}\boldsymbol{I}V + V^{-1}\left(\widehat{J}-\widetilde{J}\right)\left(\widehat{J}+\widetilde{J}\right)V\right],\end{aligned} \tag{2.105}$$

$$\begin{aligned}\mathring{\mathcal{S}}(\mu) :&= -i\mu\Lambda_P - \mu^2\mathring{\mathcal{E}}_P \\ &= -i\mu\Lambda_P - \xi^2\left[K^{-1}\frac{\ell^*\Delta x}{2}\boldsymbol{I}K + K^{-1}\left(\widehat{P}-\widetilde{P}\right)\left(\widehat{P}+\widetilde{P}\right)K\right],\end{aligned} \tag{2.106}$$

where

$$\mathring{\mathcal{E}}_J = V^{-1}D_J V, \qquad \mathring{\mathcal{E}}_P = K^{-1}D_P K. \tag{2.107}$$

Since $\mathring{\mathcal{P}}(\xi)$ and $\mathring{\mathcal{S}}(\mu)$ are both the sum of a Hermitian and a skew-Hermitian matrix, respectively, one can use Theorem II in [2], which demonstrates that the sum will have stable eigenvalues, i.e., the eigenvalues have negative real parts, if providing a Hermitian matrix with stable eigenvalues in the left half-plane and a skew-Hermitian matrix.

Accordingly, the positivity of $\mathring{\mathcal{E}}_J$ and $\mathring{\mathcal{E}}_P$ are sufficient to guarantee that $\mathcal{P}(\xi)$ and $\mathcal{S}(\mu)$ only have eigenvalues with negative real parts. If the real part of these eigenvalues is uniformly bounded, it implies the modified equation (2.102) is L_2-stable according to [35].

Moreover, one can study

$$\mathring{\mathcal{E}}_J^* := V^{-1}\left(\widehat{J}-\widetilde{J}\right)\left(\widehat{J}+\widetilde{J}\right)V, \tag{2.108}$$

$$\mathring{\mathcal{E}}_P^* := K^{-1}\left(\widehat{P}-\widetilde{P}\right)\left(\widehat{P}+\widetilde{P}\right)K \tag{2.109}$$

instead of $\mathring{\mathcal{E}}_J$ and $\mathring{\mathcal{E}}_P$ based on Lemma 4.1 in [52] which are extended to the current studied system as follows.

LEMMA 2.4. *Considering the system* (2.96)*, let V be the matrix of the eigenvectors of J and E be the matrix of the eigenvectors of P, and suppose that the splitting $J = \widetilde{J}+\widehat{J}$ and $P = \widetilde{P}+\widehat{P}$ are admissible. If there exists a lower-bound $\underline{\lambda}_{\mathcal{H}(\mathring{\mathcal{E}}_J^*)}$ for the eigenvalues of the Hermitian part of $\mathring{\mathcal{E}}_J^*$ and a lower-bound $\underline{\lambda}_{\mathcal{H}(\mathring{\mathcal{E}}_P^*)}$ for the eigenvalues of the Hermitian part of $\mathring{\mathcal{E}}_P^*$ such that $\underline{\lambda}_{\mathcal{H}(\mathring{\mathcal{E}}_J^*)} = \mathcal{O}(1)$ and $\underline{\lambda}_{\mathcal{H}(\mathring{\mathcal{E}}_P^*)} = \mathcal{O}(1)$, then the splitting is strictly stable in the sense of Majda and Pego* [35].

Assuming that the studied system (2.96) has been linearized around an arbitrarily fixed state, in light of Lemma 2.4, one has to study the positivity of $\mathring{\mathcal{E}}_J^*$ and $\mathring{\mathcal{E}}_P^*$. The eigenvalues of the Hermitian part of $\mathring{\mathcal{E}}_J^*$ and $\mathring{\mathcal{E}}_P^*$ in the low Froude number limit are

$$\lim_{\varepsilon\to 0}\left(\varepsilon^2\lambda^{1,2,3}_{\mathcal{H}(\mathring{\mathcal{D}}^*_J)}\right) = \lim_{\varepsilon\to 0}\left[\varepsilon^2\frac{(\alpha-2)(hu)^2}{(\eta-B)^2} + (a-B) - (\eta-B)\beta \pm (\alpha\eta-\eta+a-B\alpha), -\varepsilon^2\frac{(hu)^2}{(\eta-B)^2}\right] = \lim_{\varepsilon\to 0}\left[(a-B)\pm(a-\eta)-(\eta-B)(\alpha\pm\alpha), 0\right]. \tag{2.110}$$

$$\lim_{\varepsilon\to 0}\left(\varepsilon^2\lambda^{1,2,3}_{\mathcal{H}(\mathring{\mathcal{D}}^*_P)}\right) = \lim_{\varepsilon\to 0}\left[\varepsilon^2\frac{(\alpha-2)(hv)^2}{(\eta-B)^2} + (a-B) - (\eta-B)\beta \pm (\alpha\eta-\eta+a-B\beta), -\varepsilon^2\frac{(hv)^2}{(\eta-B)^2}\right] \tag{2.111}$$

$$= \lim_{\varepsilon\to 0}\left[(a-B)\pm(a-\eta)-(\eta-B)(\alpha\pm\alpha), 0\right]. \tag{2.112}$$

Owing to the formal analysis (2.6) and (2.3) for $\varepsilon \ll 1$, $\alpha = \varepsilon^2$ and (2.22), i.e., $(\eta - a) = \mathcal{O}(\varepsilon^2)$, (2.110) and (2.111) are simplified to

$$\lim_{\varepsilon\to 0}\left(\varepsilon^2\lambda^{1,2,3}_{\mathcal{H}(\mathring{\mathcal{D}}^*_J)}\right) = \lim_{\varepsilon\to 0}\left(\varepsilon^2\lambda^{1,2,3}_{\mathcal{H}(\mathring{\mathcal{D}}^*_P)}\right) = \begin{cases} \eta - B, \\ (a-B) - 2\alpha(\eta-B), \\ 0. \end{cases} \tag{2.113}$$

Thus, providing that

$$\alpha \le \frac{1}{2}\min_{j,k}\left(\frac{a-B}{\eta-B}\right), \tag{2.114}$$

all the eigenvalues (2.113) are nonnegative, and the lower-bound $\underline{\lambda}_{\mathcal{H}(\mathring{\mathcal{D}}^*_J)} = \underline{\lambda}_{\mathcal{H}(\mathring{\mathcal{D}}^*_P)} = \mathcal{O}(1)$. Due to Lemma 2.4, the proposed IMEX flux splitting approach is strictly stable in the sense of Majda and Pego [35] and no extra stability restriction is introduced. Therefore, the proposed numerical scheme is uniformly stable when the CFL condition (2.23) for the explicit part is satisfied.

Notice that $\alpha = \varepsilon^2$ generally satisfy (2.114) for the low Froude number flows. When ε becomes large, the value of α is restricted by (2.114).

3. Numerical examples. This section investigates the performance of the proposed AP scheme on several numerical examples.

In the numerical tests in subsections 3.2, 3.5, and 3.6, a second order fully explicit shock capturing finite volume method is adopted for comparison. Such explicit schemes solve the governing system (1.4) using a second order Rusanov approximation for fluxes as described in subsection 2.4.2 and a central differencing scheme (2.24) for the bed-slope source terms. In order to obtain the second order accuracy in time, the strong-stability-preserving two-staged Runge–Kutta method in [19] is applied to the explicit scheme. To ensure the stability of the explicit scheme, the time step size is restricted by (1.5).

3.1. Example 1—Quiescent water over a hump. In this test, the well-balanced property of the proposed numerical scheme is verified by simulating the "lake at rest" steady state defined by

$$\eta(x,y,0) = 6, \quad u(x,y,0) = v(x,y,0) = 0,$$

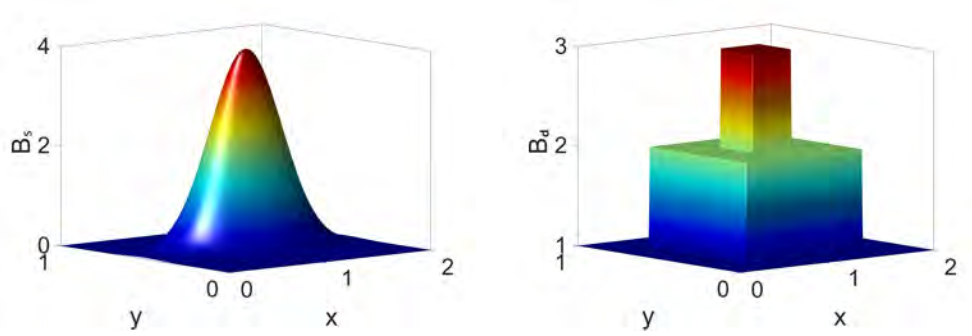

FIG. 2. *Example* 1: *Smooth (left) and discontinuous (right) bottom topography.*

TABLE 1

Example 1: *Errors between the exact and numerical solutions at* $t = 5$ *with different* ε *over smooth* (B_s) *and discontinuous* (B_d) *beds.*

Bottom	η		u		v	
$\varepsilon = 0.05$						
	L^1-error	L^∞-error	L^1-error	L^∞-error	L^1-error	L^∞-error
B_s	$2.39e{-}15$	$1.07e{-}14$	$8.94e{-}12$	$6.76e{-}11$	$9.70e{-}12$	$6.15e{-}11$
B_d	$1.81e{-}15$	$7.99e{-}15$	$3.92e{-}12$	$4.83e{-}11$	$4.41e{-}12$	$4.31e{-}11$
$\varepsilon = 0.8$						
	L^1-error	L^∞-error	L^1-error	L^∞-error	L^1-error	L^∞-error
B_s	$2.07e{-}15$	$1.06e{-}14$	$5.17e{-}14$	$3.20e{-}13$	$4.92e{-}14$	$2.60e{-}13$
B_d	$1.73e{-}15$	$8.8e{-}15$	$2.70e{-}14$	$4.99e{-}13$	$5.98e{-}14$	$4.91e{-}13$

over a smooth(B_s) and a discontinuous(B_d) topography defined by

$$B_s(x,y) = 4\exp\left[-5(x-1)^2 - 50(y-0.5)^2\right]$$

and

$$B_d(x,y) = \begin{cases} 3 & \text{if} \quad 0.8 < x < 1.2 \quad \text{and} \quad 0.4 < y < 0.6, \\ 2 & \text{if} \quad 0.4 \le x \le 1.6 \quad \text{and} \quad 0.2 \le y \le 0.8, \\ 1 & \text{otherwise}, \end{cases}$$

respectively; see Figure 2.

The $[0,2] \times [0,1]$ computational domain is divided by a coarse mesh with 40×20 uniform cells, and a periodic boundary condition is applied to all the boundaries. The "lake at rest" steady state is simulated until $t = 5$ for $\varepsilon = 0.05$ and $\varepsilon = 0.8$, respectively.

Table 1 shows the errors between the exact and numerical solutions at $t = 5$ with different ε over both smooth and a discontinuous bottom topography. One can see that the computed variables remain constant only with very small errors which are basically the same magnitude as machine errors. It demonstrates that the proposed AP scheme is well-balanced and able to preserve the "lake at rest" steady-state solutions.

3.2. Example 2—Traveling vortex over a flat bed. This test investigates the performance of the proposed numerical scheme modeling a traveling vortex propagating over a flat bed. An analytical solution to the two-dimensional SWEs for the

traveling vortex was demonstrated in [40] and used in [3, 45]. The analytical solution is used to verify the EOC of the proposed AP scheme in this test.

The computational domain is a square region $[0,1]\times[0,1]$ divided into $N\times N$ uniform structured cells. The periodic boundary conditions are applied to all the boundaries. The following initial conditions are adopted:

$$\eta(x,y,0) = 110 + \begin{cases} \left(\dfrac{\varepsilon\Gamma}{\omega}\right)^2 \big[k(\omega r) - k(\pi)\big] & \text{if } \omega r \le \pi, \\ 0 & \text{otherwise,} \end{cases}$$

$$u(x,y,0) = 0.6 + \begin{cases} \Gamma\big[1+\cos(\omega r)\big](0.5-y) & \text{if } \omega r \le \pi, \\ 0 & \text{otherwise,} \end{cases}$$

$$v(x,y,0) = \begin{cases} \Gamma\big[1+\cos(\omega r)\big](x-0.5) & \text{if } \omega r \le \pi, \\ 0 & \text{otherwise,} \end{cases}$$

$$r = \sqrt{(x-0.5)^2+(y-0.5)^2}, \quad \Gamma = 8, \quad \omega = 4\pi,$$

$$k(\zeta) = 2\cos(\zeta) + 2r\sin(\zeta) + \frac{1}{8}\cos(2\zeta) + \frac{\zeta}{4}\sin(2r) + \frac{3}{4}\zeta^2.$$

Using the above-defined initial condition, a rotating vortex initially located at the domain center $(0.5, 0.5)$ is transported repeatedly from left to right with a period $T = 5/3$ by an x-directional uniform flow. The analytical solution at any time t is given by

$$\begin{aligned} \eta(x,y,t) &= \eta(x - t/T, y, 0), \\ u(x,y,t) &= u(x - t/T, y, 0), \\ v(x,y,t) &= v(x - t/T, y, 0). \end{aligned} \tag{3.1}$$

In Figure 3, numerical results computed by the explicit and proposed AP schemes for $\varepsilon = 3$, 1, 0.1, and 0.01, respectively, using 80×80 mesh cells are shown. It demonstrates that with different ε the proposed AP schemes preserve the position and amplitude of the traveling vortex very well in different flow regimes, whereas the explicit schemes are more diffusive and completely dominated by the numerical diffusion in the low Froude number regimes. Moreover, in Table 2 for the CPU time consumed by both the explicit and proposed AP schemes, one can clearly observe huge computational savings for the AP scheme in the low Froude regime.

Figure 4 shows that the proposed AP scheme can stably and accurately predict the flow discharges for both large and small Froude numbers.

We then verify the experimental order of convergence (EOC) of the proposed AP scheme in different flow regimes. The EOC is computed using the formula

$$\mathrm{EOC} = \log\left(\frac{N_2 \sum\limits_{j,k} \big\|\zeta_1 - \zeta_{\mathrm{exact}}\big\|}{N_1 \sum\limits_{j,k} \big\|\zeta_2 - \zeta_{\mathrm{exact}}\big\|}\right) \Big/ \log\left(\frac{N_2}{N_1}\right),$$

where the subscripts 1 and 2 represent different mesh sizes for numerical approximation. The numerical solutions and exact solutions are obtained at time $t = T$ for different ε values. It is shown in Table 3 the measured L^1-error of primitive variables η, hu, and hv and the EOC with different grid numbers $N\times N$. The obtained results confirm the second order accuracy of the proposed AP schemes.

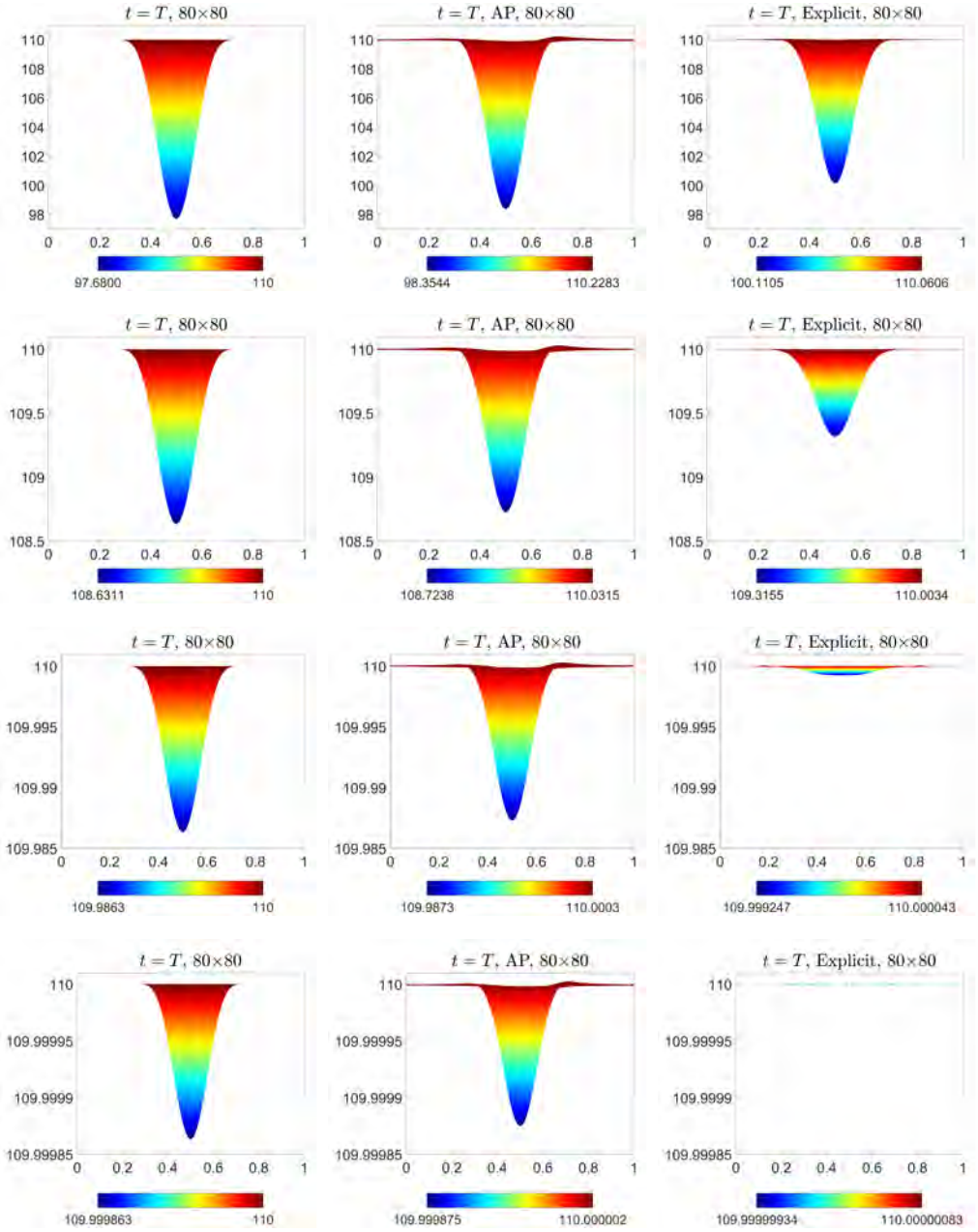

FIG. 3. *Example* 2: *Side view of* η *computed by the AP and explicit schemes for* $\varepsilon = 3$ *(first row),* $\varepsilon = 1$ *(second row),* $\varepsilon = 0.1$ *(third row),* $\varepsilon = 0.01$ *(fourth row) using* 80×80 *grids at* $t = T$.

TABLE 2

Example 2: *CPU times consumed by the AP and explicit schemes on* 80×80 *grids for different values of* ε *at* $t = T$.

$\varepsilon = 3$		$\varepsilon = 1$		$\varepsilon = 0.1$		$\varepsilon = 0.01$	
AP	Explicit	AP	Explicit	AP	Explicit	AP	Explicit
6.46 s	10.03 s	8.59 s	20.51 s	80.12 s	178.98 s	178.64 s	1571.72 s

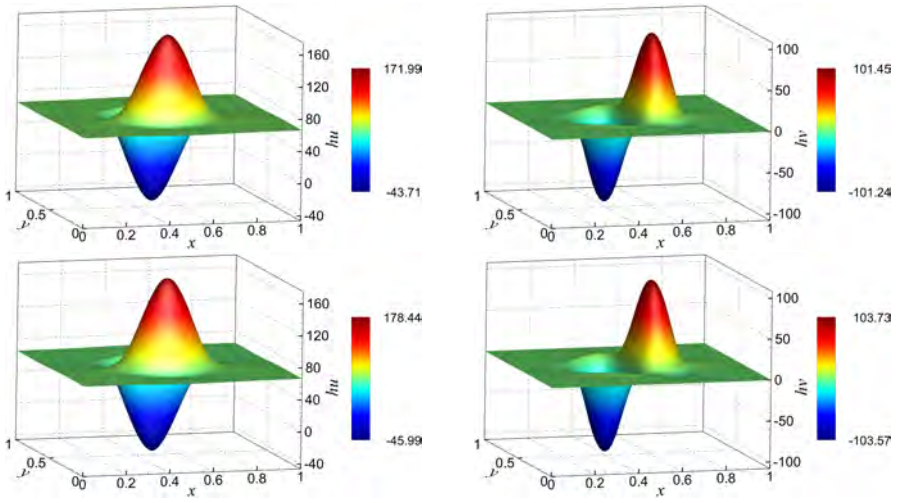

FIG. 4. *Example* 2: *Computed flow discharges by the proposed AP schemes for* $\varepsilon = 3$ *(first row),* $\varepsilon = 0.01$ *(second row) using* 80×80 *grids at* $t = T$.

TABLE 3
Example 2: L^1*-errors and EOC for different* ε.

$\varepsilon = 1$, $\text{CFL}_{AP} = 0.6$, $\text{CFL} \approx 2.3$, $t = T$

N	L^1-error in η	EOC	L^1-error in hu	EOC	L^1-error in hv	EOC
40	3.38×10^{-2}	—	4.51	—	4.34	—
80	1.10×10^{-2}	1.62	1.57	1.52	1.50	1.53
120	4.91×10^{-3}	1.99	0.79	1.70	0.69	1.92
160	2.09×10^{-3}	2.97	0.36	2.73	0.32	2.67
200	1.12×10^{-3}	2.79	0.21	2.42	0.20	2.11

$\varepsilon = 0.1$, $\text{CFL}_{AP} = 0.6$, $\text{CFL} \approx 23.4$, $t = T$

N	L^1-error in η	EOC	L^1-error in hu	EOC	L^1-error in hv	EOC
40	2.02×10^{-3}	—	4.56	—	4.38	—
80	1.14×10^{-4}	4.15	1.60	1.51	1.54	1.51
120	4.83×10^{-5}	2.12	0.79	1.74	0.69	1.98
160	2.01×10^{-5}	3.04	0.36	2.73	0.32	2.67
200	1.05×10^{-5}	2.91	0.22	2.21	0.20	2.11

$\varepsilon = 0.01$, $\text{CFL}_{AP} = 0.6$, $\text{CFL} \approx 231.8$, $t = T$

N	L^1-error in η	EOC	L^1-error in hu	EOC	L^1-error in hv	EOC
40	1.72×10^{-4}	—	4.55	—	4.37	—
80	5.71×10^{-6}	4.91	1.60	1.51	1.53	1.51
120	9.35×10^{-7}	4.46	0.79	1.74	0.69	1.96
160	3.48×10^{-7}	3.43	0.36	2.73	0.32	2.67
200	2.15×10^{-7}	2.16	0.22	2.21	0.20	2.11

3.3. Example 3—Traveling vortex over an irregular bed. This test investigates the performance of the proposed AP schemes in the low Froude number limit over an irregular bottom. To this end, the following irregular bottom topography is added to the numerical experiment in subsection 3.2:

$$B(x, y) = 10 \exp\left[-5(x-1)^2 - 50(y-0.5)^2\right].$$

Moreover, $\varepsilon = 0.05$ is set in this test.

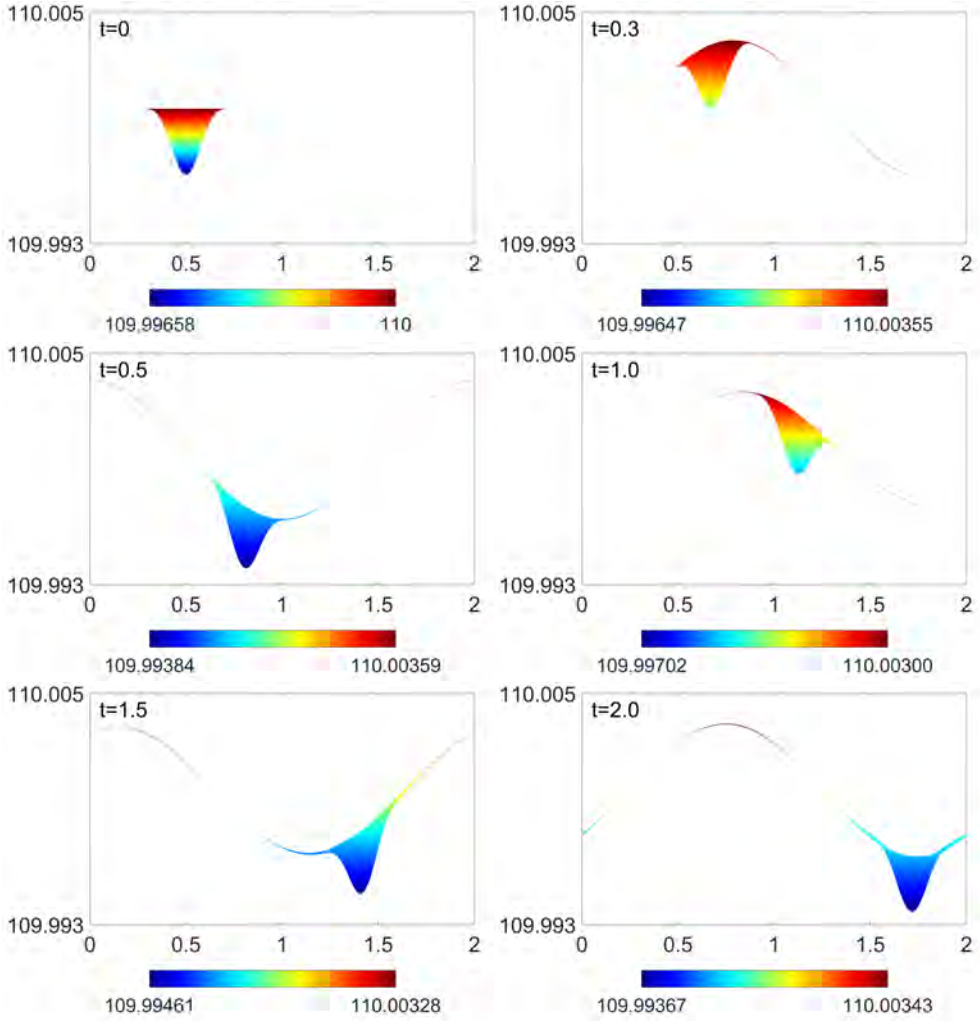

FIG. 5. *Example* 3: *Side view of* η *computed by the proposed AP schemes for* $\varepsilon = 0.05$ *using* 160×80 *grids at different times.*

Figure 5 shows the side views of η, while Figure 6 shows the contour lines of surface level η computed by the proposed AP schemes at different times. One can observe periodic sine-type waves generated due to the irregular bottom, and the structure of the vortex traveling with the waves is well-preserved during the simulation.

3.4. Example 4—Sine wave evolution. This numerical experiment studies the performance of the proposed AP scheme modeling a small amplitude sine wave transportation in the small Froude number regimes. Following [12], the initial conditions are defined by

$$\begin{aligned} \eta(x,y,0) &= 1 + \varepsilon^2 \sin^2\left[2\pi(x+y)\right] \\ hu(x,y,0) &= \sin^2\left[2\pi(x-y)\right] + \varepsilon^2 \sin^2\left[2\pi(x+y)\right] \\ hv(x,y,0) &= \sin^2\left[2\pi(x-y)\right] + \varepsilon^2 \cos^2\left[2\pi(x+y)\right] \end{aligned} \tag{3.2}$$

over a $[0,1] \times [0,1]$ square domain.

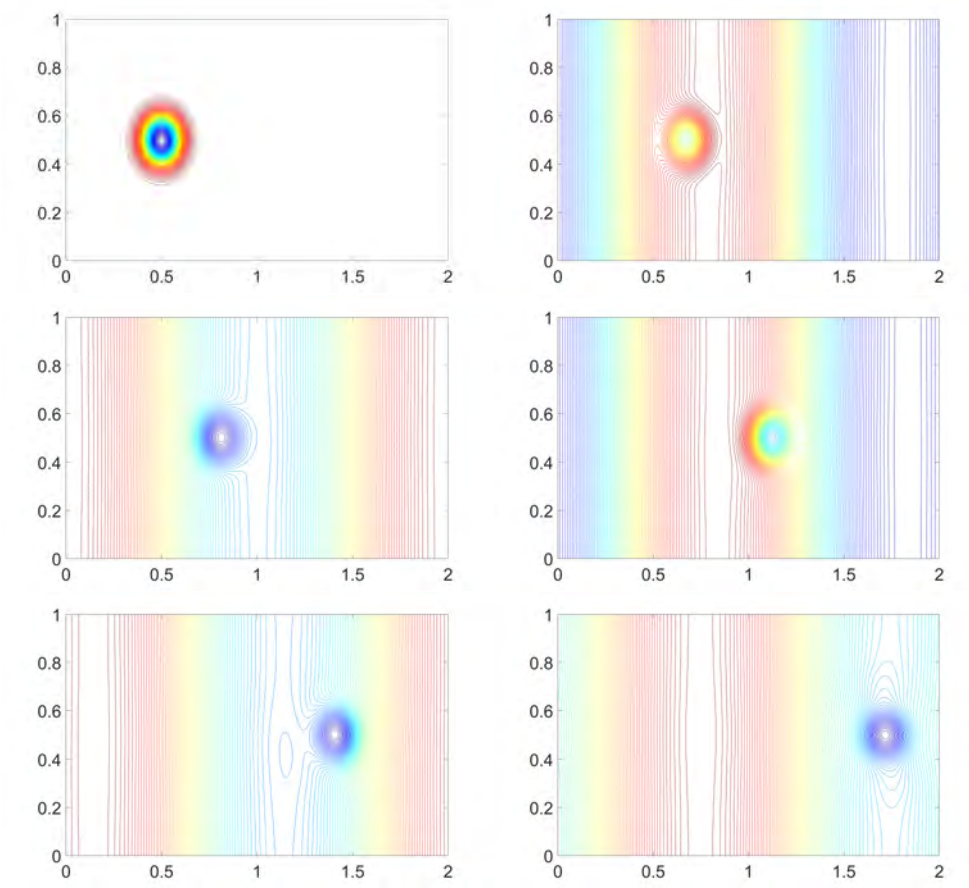

FIG. 6. *Example* 3: *Contour lines of surface level* η *computed by the proposed AP schemes for* $\varepsilon = 0.05$ *using* 160×80 *grids at* $t = 0, 0.4, 0.8, 1.2, 1.6, 2$ *(from left to right and from top to bottom).*

It is noticed that, as described in [3], although [12] provides an AP scheme for the isentropic Euler equations, one can compare the results of homogeneous SWEs in this test with the results in [12] when identifying the water depth h with the gas density ρ and setting the equation of state for compressible gas to be $p(\rho) := \frac{1}{2}\rho^2$.

The computational domain is discretized by 160×160 uniform grids, and periodic boundary conditions are applied to all the boundaries. The computed results are obtained at $t = 1$ using $\varepsilon = 0.05$ and 0.005.

Figure 7 shows the numerical solutions of the proposed schemes with $\varepsilon = 0.05$; one can observe that the proposed numerical model captures the small wave perturbations well, and the magnitude and contour of flow discharges remain nearly constant during the simulation. The results are analogous to those in [12]. Figure 8 shows that the numerical solutions of the proposed schemes with $\varepsilon = 0.005$ and demonstrates that the proposed numerical schemes capture the flow details accurately in this very small Froude number limit. One can also observe that $(hu)_x + (hv)_y$ converge to zero when $\varepsilon \to 0$ at $\mathcal{O}(\varepsilon^2)$.

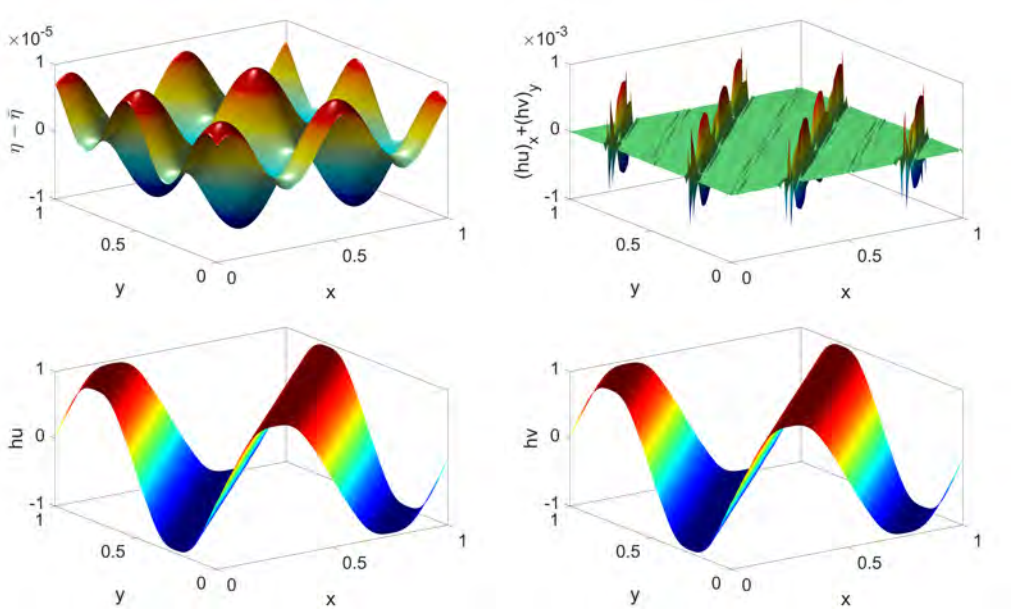

FIG. 7. *Example* 4: *Numerical solutions of the sine wave evolution computed by the proposed AP schemes for* $\varepsilon = 0.05$.

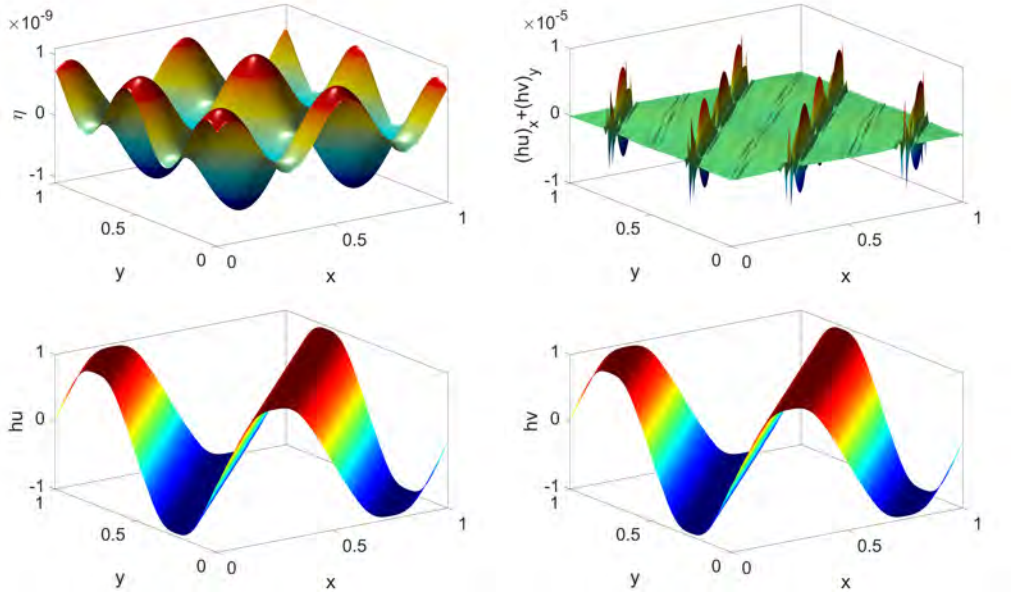

FIG. 8. *Example* 4: *Numerical solutions of the sine wave evolution computed by the proposed AP schemes for* $\varepsilon = 0.005$.

3.5. Example 5—Shock wave transportation over an irregular bottom. This test demonstrates how the proposed numerical scheme performs when modeling shock wave propagation over an irregular bottom defined by

$$B(x,y) = 2\exp\left[-2(x-1)^2\right]$$

in a $[0,2]\times[0,0.2]$ computational domain. The initial discontinuity of surface level is defined by

$$\eta(x,y,0) = 6 + \begin{cases} 0.5 & \text{if} \quad 0.6 \le x \le 1.4, \\ 0 & \text{otherwise}, \end{cases} \tag{3.3}$$

$$u(x,y,0) = v(x,y,0) = 0.$$

The computational domain is discretized by 100×10 uniform grids, and a periodic boundary condition is applied to all the boundaries.

The numerical solutions computed by the currently proposed AP scheme are compared with a second order fully explicitly shock capturing Rusanov scheme in the following with $\varepsilon = 0.05$ and $\varepsilon = 0.9$, respectively. We consider the following three tests over the same mesh with different time step size for the proposed AP schemes.

Notice that the solutions of the fully explicit method are computed with the maximum (approximately) Δt_{ex} allowed by (1.5) over the same mesh.

Test (I). First the time step size for the proposed AP scheme is chosen the same as the explicit shock capturing scheme, i.e., $\Delta t_{AP} = \Delta t_{ex} = 2\times 10^{-4}$ with $\varepsilon = 0.05$, and $\Delta t_{AP} = \Delta t_{ex} = 2\times 10^{-3}$ with $\varepsilon = 0.9$.

The comparisons of the solutions in Figure 9 show that the propagated shock waves are well-captured by both schemes with such time step sizes.

Test (II). Next, the performance of the proposed AP scheme with larger time step size over the same discretized mesh is investigated. Under the restriction (2.23),

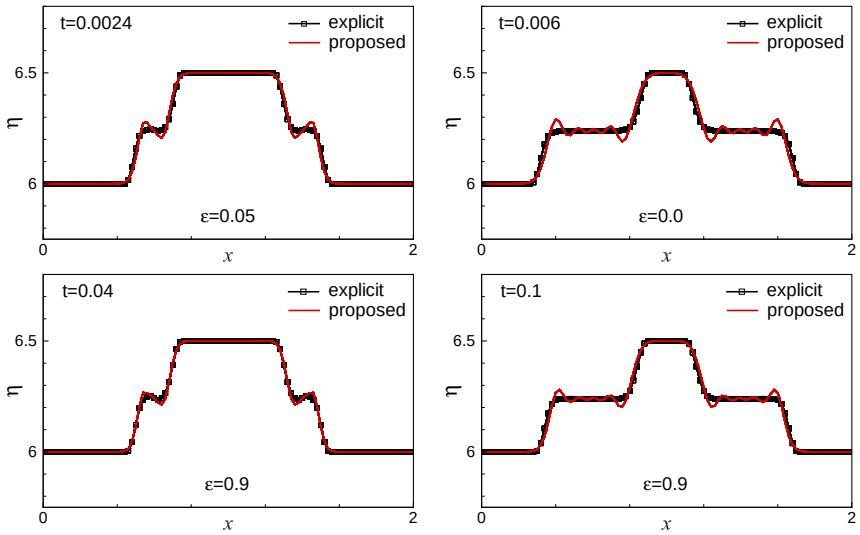

FIG. 9. *Example* 5: *Test* (I) *($\Delta t_{AP} = \Delta t_{ex}$). Shock wave propagation with $\varepsilon = 0.05$ and $\varepsilon = 0.9$, respectively, at different times.*

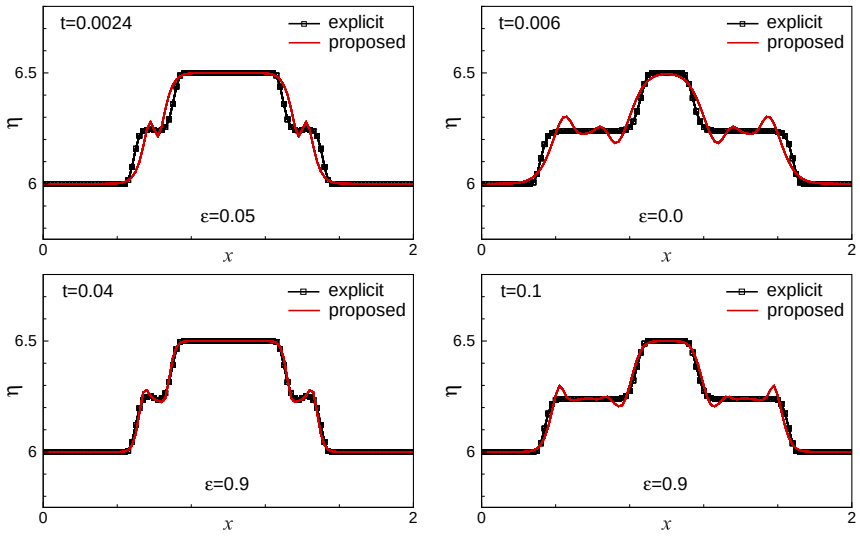

FIG. 10. *Example* 5: *Test* (II) ($\Delta t_{AP} = 10\Delta t_{ex}$). *Shock wave propagation with* $\varepsilon = 0.05$ *and* $\varepsilon = 0.9$, *respectively, at different times.*

a time step 10 times the explicit time step size for the proposed AP scheme, i.e., $\Delta t_{AP} = 10\,\Delta t_{ex} = 2 \times 10^{-3}$ for the case $\varepsilon = 0.05$ and $\Delta t_{AP} = 10\,\Delta t_{ex} = 2 \times 10^{-2}$ for the case $\varepsilon = 0.9$. The solutions of the proposed AP scheme with such time step sizes are compared with the fully explicit shock capturing Rusanov schemes in Figure 10.

One can see that the proposed AP scheme can capture the shock wave propagation well with large ε. For the low Froude number flows with $\varepsilon = 0.05$, the proposed AP scheme can well capture the position and height of the shock wave fronts compared with the explicit shock capturing scheme.

Test (III). Finally, the maximum time step size allowed by the proposed AP scheme is used to compute the final solutions over the same discretized mesh. With low Froude number $\varepsilon = 0.05$, only one time step is required to obtain the final solution at $t = 0.006$, i.e., $\Delta t_{AP} = 30\,\Delta t_{ex} = 6 \times 10^{-3}$. With large Froude number $\varepsilon = 0.9$, four time steps are required to obtain the final solution at $t = 0.1$, i.e., $\Delta t_{AP} = 12.5\,\Delta t_{ex} = 2.5 \times 10^{-2}$.

Figure 11 shows the solutions of the proposed AP scheme with such time step sizes in comparison with the explicit shock capturing schemes. Due to the relative restrictive limitation of Δt_{AP} for large Froude number $\varepsilon = 0.9$, approximately the same Δt_{AP} as that in Test (II) is used; therefore the proposed scheme captures the shock wave propagation similarly as that in Test (II). However, for the low Froude number flows with $\varepsilon = 0.05$, with such a large time step size ($30\,\Delta t_{ex}$), the proposed AP scheme introduces more dispersion to distort and damp the gravity waves not well-resolved in time and thus does not capture the shock wave fronts.

3.6. Example 6—Multiscale test. In this test, the performance of the currently proposed AP scheme when solving multiscale waves is demonstrated.

To this end, the test in [29] is modified here and the initial data for this test is given by

$$\eta(x, y, 0) = 1 + \frac{\sigma(x)}{2}\sin(\varepsilon 40\pi x) + \varepsilon\big[1 + \cos(\varepsilon\pi x)\big],$$

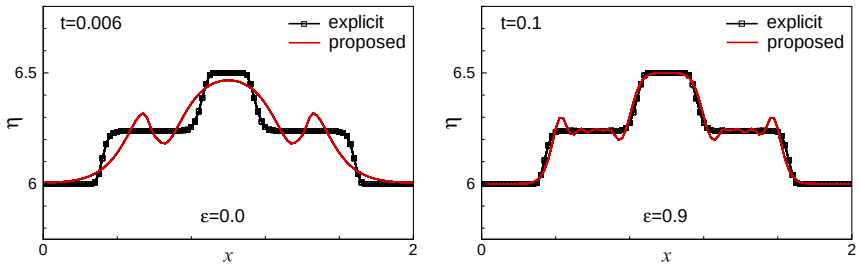

FIG. 11. *Example* 5: *Test* (III) ($\Delta t_{AP} = \Delta t_{AP}$). *Shock wave propagation with* $\varepsilon = 0.05$ *and* $\varepsilon = 0.9$, *respectively, at different times.*

$$u(x, y, 0) = \sqrt{2}\big[1 + \cos(\varepsilon\pi x)\big],$$

where $\varepsilon = 0.02$, and the following two cases are considered:

case (a):

$$\sigma(x, y) = 0,$$

case (b):

$$\sigma(x, y) = \begin{cases} 0.5\,[1 - \cos(0.1\pi x)] & \text{if} \quad 0 \le x \le 20, \\ 0 & \text{otherwise.} \end{cases}$$

In case (a), the proposed AP scheme when modeling a problem of weakly nonlinear long wave is tested.

In case (b), a large amplitude, short wave length surface fluctuation to the case (a) is added, and the propagation of such gravity waves computed by the proposed AP scheme is demonstrated.

A $[-51, 51] \times [-0.2, 0.2]$ computational domain is discretized by 1020×4 uniform grids, and a periodic boundary condition is applied to all the boundaries.

Figure 12 shows the numerical solutions of both the proposed AP scheme and the explicit scheme for case (a). One can see that the proposed semi-implicit AP scheme preserves the amplitude of the wave and its speed very well, and the solutions of both AP and explicit scheme agree well.

Figure 13 shows the numerical solutions of both the proposed AP scheme and the explicit scheme for case (b). At the beginning of the simulation, the oscillatory surface fluctuation splits into two short-waves traveling upstream and downstream in the x-direction, respectively. The comparisons in Figure 13 clearly show that the proposed AP scheme is less dispersive than the explicit scheme and preserves the amplitude of split short-waves better. The computed wave positions of the short-waves from both AP and explicit schemes agree well. One can see that the proposed AP scheme is able to appropriately damp the highly oscillatory data underresolved by the large time step size while well resolving the long acoustic waves.

4. Conclusion. In the current study, a new well-balanced AP scheme for the 2D low Froude number shallow water flows over an irregular bottom has been developed and analyzed. Replacing water depth h by free surface level η, the governing system (1.4) is reformulated to obtain a hyperbolic balance law (2.1) the flux of which is then split into a slow dynamics and a fast dynamics. The semi-implicit approach is used to approximate the nonstiff slow dynamics part explicitly and the stiff fast dynamics part implicitly. In space, the nonstiff part is discretized using a second order finite

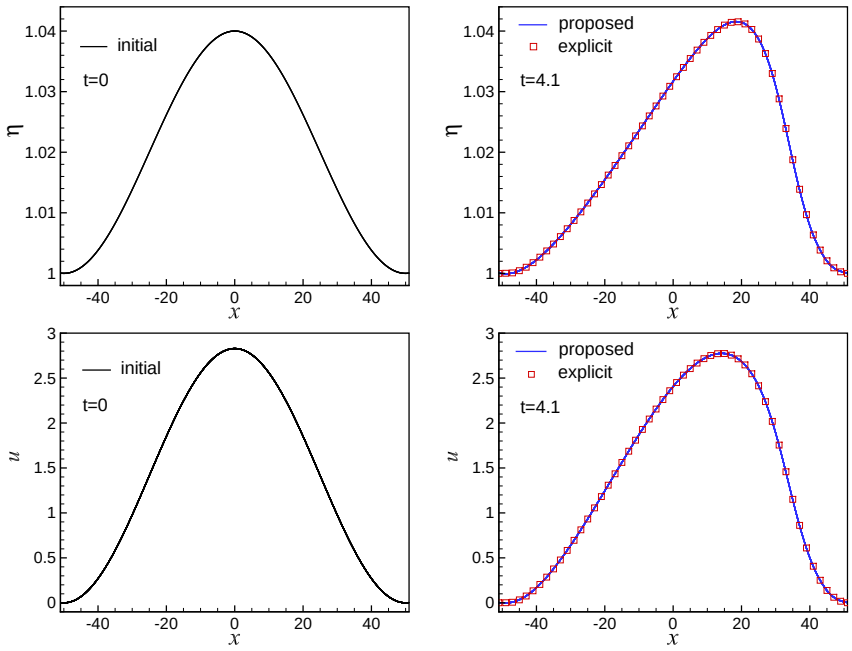

FIG. 12. *Example* 6: *case* (a). *Initial data (left) and numerical solutions of single scale longwave acoustic wave propagation at* $t = 4.1$ *(right) by the AP (CFL* ≈ 6.3*) and explicit (CFL* $= 0.4$*) schemes.*

volume Rusanov method and the stiff part is discretized using a second order central difference method. For time evolution, a second order globally stiffly accurate IMEX scheme ARS(2,2,2) is adopted. Thus, a second order accurate semi-implicit numerical scheme is successfully built.

In subsection 2.7, it is proved that the reformulated governing system (2.1) and AP schemes will guarantee the well-balanced property and preserve the "lake at rest" steady-state solutions. The experiment in subsection 3.1 numerically proves such a property of the scheme.

In susections 2.8 and 2.9, it has been proved that the proposed numerical scheme is uniformly consistent, stable, and efficient for any $0 < \varepsilon \ll 1$. Thus, the proposed IMEX scheme is asymptotic preserving and allows one to use large time step size when $\varepsilon \to 0$. This significantly increase the computational efficiency comparing with the explicit method. Numerical examples presented in the paper clearly demonstrate that the proposed AP scheme yields efficient, accurate, and stable approximation for the low Froude number 2D shallow water flows over irregular beds.

The CFL number of gravity wave τ is $\mathcal{O}(\frac{\Delta t}{\varepsilon \Delta x})$, and $\tau \gg 1$ in the limit $\varepsilon \to 0$. Applying implicit discretization to the gravity wave terms successfully gets rid of such stability restrictions from the CFL number τ of gravity waves and provides the stability of the IMEX scheme limited only by the advective CFL condition (2.23) which is independent on ε. This thus allows for a much larger time step size in the low Froude number flow regime. However, such a large time step AP scheme may distort and damp the fast gravity wave solutions which are not well-resolved by the used large time step Δt_{AP}, until they satisfy the advective CFL condition (2.23). See the results of the numerical experiments in subsections 3.5 and 3.6.

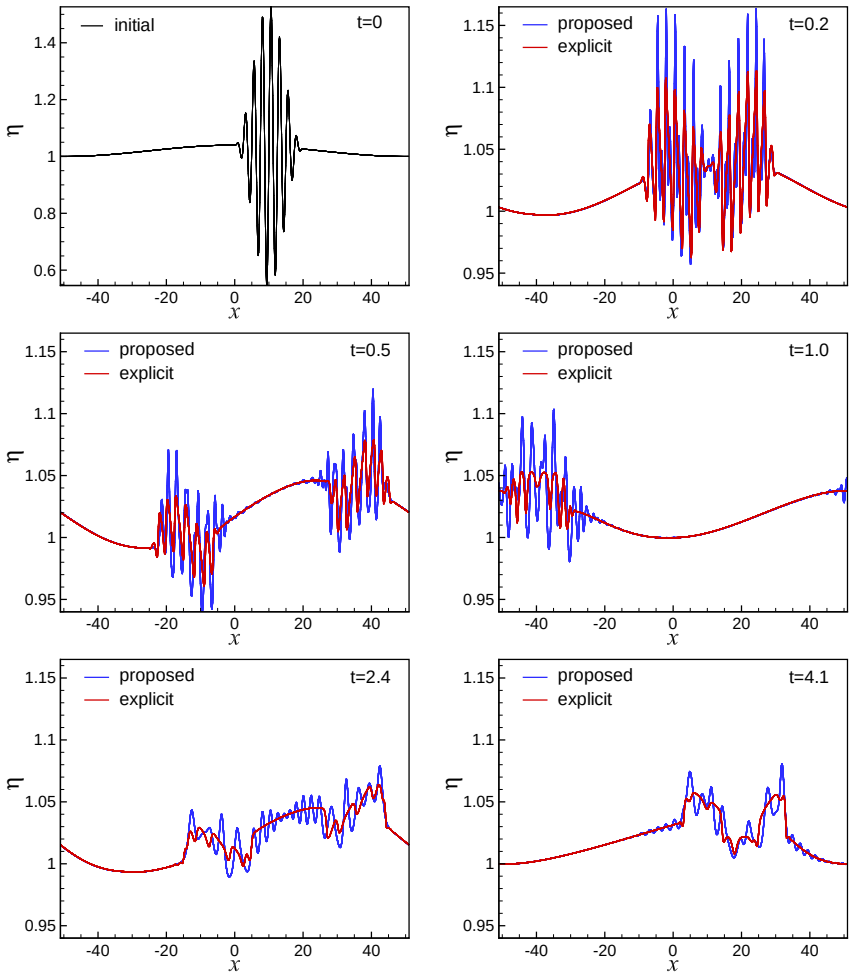

FIG. 13. *Example* 6: *case* (b). *Numerical solutions of multiscale wave propagation by the AP (CFL* ≈ 5.4*) and explicit (CFL* $= 0.4$*) schemes.*

This is an acceptable distortion since the author is more interested in the "current-like" slow processes and asymptotically preserving the wave structures in the scale resolved by the dimensionless coordinate x as claimed in Remark 1.1. Asymptotically preserving such fast gravity waves along with the currently proposed asymptotic preserving schemes will be the author's next step.

REFERENCES

[1] U. M. ASCHER, S. J. RUUTH, AND R. J. SPITERI, *Implicit-explicit Runge-Kutta methods for time-dependent partial differential equations*, Appl. Numer. Math., 25 (1997), pp. 151–167.

[2] I. BENDIXSON, *Sur les racines d'une équation fondamentale*, Acta Math., 25 (1902), pp. 359–365.

[3] G. BISPEN, K. R. ARUN, M. LUKÁČOVÁ-MEDVIĎOVÁ, AND S. NOELLE, *IMEX large time step finite volume methods for low Froude number shallow water flows*, Commun. Comput. Phys., 16 (2014), pp. 307–347.

[4] G. Bispen, M. Lukáčová-Medvid'ová, and L. Yelash, *Asymptotic preserving imex finite volume schemes for low Mach number Euler equations with gravitation*, J. Comput. Phys., 335 (2017), pp. 222–248.
[5] S. Boscarino, G. Russo, and L. Scandurra, *All mach number second order semi-implicit scheme for the euler equations of gas dynamics*, J. Sci. Comput., 77 (2018), pp. 850–884.
[6] D. Bresch, R. Klein, and C. Lucas, *Multiscale analyses for the shallow water equations*, in Computational Science and High Performance Computing IV, Springer, New York, 2011, pp. 149–164.
[7] F. Cordier, P. Degond, and A. Kumbaro, *An asymptotic-preserving all-speed scheme for the Euler and Navier-Stokes equations*, J. Comput. Phys., 231 (2012), pp. 5685–5704.
[8] F. Couderc, A. Duran, and J.-P. Vila, *An explicit asymptotic preserving low Froude scheme for the multilayer shallow water model with density stratification*, J. Comput. Phys., 343 (2017), pp. 235–270.
[9] P. Crispel, P. Degond, and M.-H. Vignal, *An asymptotic preserving scheme for the two-fluid Euler–Poisson model in the quasineutral limit*, J. Comput. Phys., 223 (2007), pp. 208–234.
[10] R. Danchin, *Low Mach number limit for viscous compressible flows*, ESAIM Math. Model. Numer. Anal., 39 (2005), pp. 459–475.
[11] P. Degond, F. Deluzet, A. Sangam, and M.-H. Vignal, *An asymptotic preserving scheme for the Euler equations in a strong magnetic field*, J. Comput. Phys., 228 (2009), pp. 3540–3558.
[12] P. Degond and M. Tang, *All speed Scheme for the low Mach number limit of the isentropic Euler equations*, Commun. Comput. Phys., 10 (2011), pp. 1–31.
[13] S. Dellacherie, P. Omnes, and F. Rieper, *The influence of cell geometry on the Godunov scheme applied to the linear wave equation*, J. Comput. Phys., 229 (2010), pp. 5315–5338.
[14] G. Dimarco, R. Loubère, and M.-H. Vignal, *Study of a new asymptotic preserving scheme for the Euler system in the low Mach number limit*, SIAM J. Sci. Comput., 39 (2017), pp. A2099–A2128.
[15] A. Duran, F. Marche, R. Turpault, and C. Berthon, *Asymptotic preserving scheme for the shallow water equations with source terms on unstructured meshes*, J. Comput. Phys., 287 (2015), pp. 184–206.
[16] F. X. Giraldo, J. F. Kelly, and E. M. Constantinescu, *Implicit-explicit formulations of a three-dimensional nonhydrostatic unified model of the atmosphere (NUMA)*, SIAM J. Sci. Comput., 35 (2013), pp. B1162–B1194.
[17] F. X. Giraldo and M. Restelli, *High-order semi-implicit time-integrators for a triangular discontinuous Galerkin oceanic shallow water model*, Internat. J. Numer. Methods Fluids, 63 (2010), pp. 1077–1102.
[18] F. X. Giraldo, M. Restelli, and M. Läuter, *Semi-implicit formulations of the Navier–Stokes equations: Application to nonhydrostatic atmospheric modeling*, SIAM J. Sci. Comput., 32 (2010), pp. 3394–3425.
[19] S. Gottlieb, C. W. Shu, and E. Tadmor, *Strong stability-preserving high-order time discretization methods*, SIAM Rev., 43 (2001), pp. 89–112.
[20] H. Guillard and A. Murrone, *On the behavior of upwind schemes in the low Mach number limit:* II. *Godunov type schemes*, Comput. & Fluids, 33 (2004), pp. 655–675.
[21] H. Guillard and C. Viozat, *On the behaviour of upwind schemes in the low Mach number limit*, Comput. & Fluids, 28 (1999), pp. 63–86.
[22] J. Haack, S. Jin, and J.-G. Liu, *An all-speed asymptotic-preserving method for the isentropic Euler and Navier-Stokes equations*, Commun. Comput. Phys., 12 (2012), pp. 955–980.
[23] J. Hu, S. Jin, and Q. Li, *Asymptotic-preserving schemes for multiscale hyperbolic and kinetic equations*, in Handbook of Numerical Methods for Hyperbolic Problems, Handb. Numer. Anal. 18, Elsevier/North-Holland, Amsterdam, 2017, pp. 103–129.
[24] S. Jin, *Efficient asymptotic-preserving (AP) schemes for some multiscale kinetic equations*, SIAM J. Sci. Comput., 21 (1999), pp. 441–454.
[25] S. Jin, *Asymptotic preserving (AP) schemes for multiscale kinetic and hyperbolic equations: A review*, Riv. Mat. Univ. Parma, 3 (2012), pp. 177–2016.
[26] S. Jin, L. Pareschi, and G. Toscani, *Uniformly accurate diffusive relaxation schemes for multiscale transport equations*, SIAM J. Numer. Anal., 38 (2000), pp. 913–936.
[27] S. Klainerman and A. Majda, *Singular limits of quasilinear hyperbolic systems with large parameters and the incompressible limit of compressible fluids*, Commun. Pure Appl. Math., 34 (1981), pp. 481–524.
[28] S. Klainerman and A. Majda, *Compressible and incompressible fluids*, Commun. Pure Appl. Math., 35 (1982), pp. 629–651.

[29] R. Klein, *Semi-implicit extension of a Godunov-type scheme based on low Mach number asymptotics,* I*: One-dimensional flow*, J. Comput. Phys., 121 (1995), pp. 213–237.
[30] R. Klein, N. Botta, T. Schneider, C.-D. Munz, S. Roller, A. Meister, L. Hoffmann, and T. Sonar, *Asymptotic adaptive methods for multi-scale problems in fluid mechanics*, in Practical Asymptotics, Springer, New York, 2001, pp. 261–343.
[31] R. Klein, E. Mikusky, and A. Owinoh, *Multiple scales asymptotics for atmospheric flows*, in Proceedings of the European Congress of Mathematics, Zürich, 2005, pp. 201–220.
[32] K.-A. Lie and S. Noelle, *On the artificial compression method for second-order nonoscillatory central difference schemes for systems of conservation laws*, SIAM J. Sci. Comput., 24 (2003), pp. 1157–1174.
[33] X. Liu, *A highly efficient numerical method for rotating oceanographic flows modeled by saint-venant system with coriolis forces*, Commun. Comput. Phys., 25 (2019), pp. 1394–1412.
[34] X. Liu, A. Chertock, and A. Kurganov, *An asymptotic preserving scheme for the two-dimensional shallow water equations with coriolis forces*, J. Comput. Phys., 391 (2019), pp. 259–279.
[35] A. Majda and R. L. Pego, *Stable viscosity matrices for systems of conservation laws*, J. Differential Equations, 56 (1985), pp. 229–262.
[36] N. Masmoudi, *Examples of singular limits in hydrodynamics*, in Handbook of Differential Equations: Evolutionary Equations, Vol. 3, Elsevier, Amsterdam, 2007, pp. 195–275.
[37] H. Nessyahu and E. Tadmor, *Nonoscillatory central differencing for hyperbolic conservation laws*, J. Comput. Phys., 87 (1990), pp. 408–463.
[38] S. Noelle, G. Bispen, K. R. Arun, M. Lukáčová-Medviďová, and C.-D. Munz, *A weakly asymptotic preserving low Mach number scheme for the Euler equations of gas dynamics*, SIAM J. Sci. Comput., 36 (2014), pp. B989–B1024.
[39] S. Noelle, G. Bispen, K. R. Arun, M. Lukáčová-Medviďová, and C.-D. Munz, *A weakly asymptotic preserving low Mach number scheme for the Euler equations of gas dynamics*, SIAM J. Sci. Comput., 36 (2014), pp. B989–B1024.
[40] M. Ricchiuto and A. Bollermann, *Stabilized residual distribution for shallow water simulations*, J. Comput. Phys., 228 (2009), pp. 1071–1115.
[41] F. Rieper, *On the dissipation mechanism of upwind-schemes in the low Mach number regime: A comparison between Roe and HLL*, J. Comput. Phys., 229 (2010), pp. 221–232.
[42] V. Rusanov, *On difference schemes of third order accuracy for nonlinear hyperbolic systems*, J. Comput. Phys., 5 (1970), pp. 507–516.
[43] S. Schochet, *The mathematical theory of low mach number flows*, ESAIM Math. Model. Numer. Anal. 39 (2005), pp. 441–458.
[44] J. Schütz and S. Noelle, *Flux splitting for stiff equations: A notion on stability*, J. Sci. Comput., 64 (2015), pp. 522–540.
[45] G. Stecca, A. Siviglia, and E. F. Toro, *A finite volume upwind-biased centred scheme for hyperbolic systems of conservation laws: Application to shallow water equations*, Commun. Comput. Phys., 12 (2012), pp. 1183–1214.
[46] P. K. Sweby, *High resolution schemes using flux limiters for hyperbolic conservation laws*, SIAM J. Numer. Anal., 21 (1984), pp. 995–1011.
[47] O. Taussky, *A recurring theorem on determinants*, Amer. Math. Monthly, 56 (1949), pp. 672–676.
[48] G. Tumolo, L. Bonaventura, and M. Restelli, *A semi-implicit, semi-lagrangian, p-adaptive discontinuous Galerkin method for the shallow water equations*, J. Comput. Phys., 232 (2013), pp. 46–67.
[49] B. van Leer, *Towards the ultimate conservative difference scheme.* V*. A second-order sequel to Godunov's method*, J. Comput. Phys., 32 (1979), pp. 101–136.
[50] S. Vater and R. Klein, *A semi-implicit multiscale scheme for shallow water flows at low froude number*, Commun. Appl. Math. Comput. Sci., 13 (2018), pp. 303–336.
[51] H. Zakerzadeh, *Asymptotic analysis of the RS-IMEX scheme for the shallow water equations in one space dimension*, ESAIM Math. Model. Numer. Anal., 53 (2019), pp. 893–924.
[52] H. Zakerzadeh and S. Noelle, *A note on the stability of implicit-explicit flux-splittings for stiff systems of hyperbolic conservation laws*, Commun. Math. Sci., 16 (2018), pp. 1–15.